

# **Assimilation of CRP Measurements for the Detection of Freezing-Thawing Process using the STEMMUS Model at Maqu Site, Tibetan Plateau**

MWANGI SAMUEL

February, 2019

SUPERVISORS:

Dr. Y. Zeng  
Prof. Dr. Z. Su

ADVISOR:

PhD. L. Yu



# **Assimilation of CRP Measurements for the Detection of Freezing-Thawing Process using the STEMMUS Model at Maqu Site, Tibetan Plateau**

MWANGI SAMUEL

Enschede, The Netherlands, February, 2019

Thesis submitted to the Faculty of Geo-Information Science and Earth Observation of the University of Twente in partial fulfilment of the requirements for the degree of Master of Science in Geo-information Science and Earth Observation.  
Specialization: Water Resources and Environmental Management

**SUPERVISORS:**

Dr. Y. Zeng  
Prof. Dr. Z. Su

**ADVISOR:**

PhD. L. Yu

**THESIS ASSESSMENT BOARD:**

Dr. Ir. S. Salama (Chair)  
Dr. C. Montzka (External Examiner, Forschungszentrum Jülich GmbH)

#### DISCLAIMER

This document describes work undertaken as part of a programme of study at the Faculty of Geo-Information Science and Earth Observation of the University of Twente. All views and opinions expressed therein remain the sole responsibility of the author, and do not necessarily represent those of the Faculty.

## ABSTRACT

---

Soil moisture (SM) is an essential component in the hydrological cycle and its observation and simulation is thus of key importance. In Maqu county, which has a frost-susceptible silty-loam soil, SM exists in vapour, liquid as well as in ice form during winter. Quantification and prediction of soil ice content (SIC) would thus play a central role in the investigation and understanding of the freezing-thawing processes in the region's hydrological ecosystem. Several SM observing methods are available at the site. These include in-situ SM probes, a cosmic ray neutron probe (CRP) and remote sensing SM satellite retrievals, which vary in their spatial scales i.e. local, medium and coarse scales, respectively. These data can be used together with land surface model forecasts with the aim of improving or updating the simulated states in data assimilation schemes that utilise Bayesian inference methods.

In this study, the CRP was recalibrated by applying soil water weighting methods based on cosmic-ray neutrons transport theory. The conventional and revised averaging methods were implemented, and the results compared with those from the previously applied uniform (equal) weighting. Results were analysed and verified against weighted soil water simulations derived using the theoretically founded COSMIC observation model where the conventional non-linear vertical method was found to give the best fit outcomes and thus selected for the calibration and subsequent averaging of SM.

The corrected neutron counts for the period under investigation were then used in observing system data assimilation experiments that utilized the particle filter with sequential importance resampling (SIR-PF) algorithm. Further to disturbed initializations in the STEMMUS-FT, model uncertainties were assumed and used in setting up the experiments with the forward neutron simulator COSMIC being used for deriving neutron counts from soil water background inputs.

It was found that with enough spread, the updated states were able to mimic the observations. In all setups, it was evident that assimilating the CRP measurements led to enhanced total soil water analyses and as a consequence, improved SIC updates. A fully coupled STEMMUS-COSMIC implementation of the SIR-PF scheme is however needed to enable holistic analysis of error propagation in the process model over time as well as allow a joint state-parameter assimilation.

**Keywords:** Soil water content, cosmic-ray neutron probe, data assimilation, STEMMUS-Freeze Thaw, Maqu Tibetan Plateau.

## ACKNOWLEDGEMENTS

---

First, I thank the Almighty God for His favour and grace in seeing me through thus far.

Sincere thanks to the Faculty ITC, University of Twente and the Dutch government through Nuffic for granting me the opportunity and enabling my study at the Institute.

Many thanks to my first supervisor, Dr. Yijian Zeng, for giving me the opportunity to undertake this interesting topic, his availability and for providing very insightful and helpful solutions to challenges faced throughout the study. I am also very grateful to my second supervisor, Prof. Bob Su, for his all-rounded wisdom and helpful guidance. To my advisor, Lianyu Yu, thank you for always being available and for your creative ideas. My supervisors' and advisor's in-depth works on land surface modelling were key in this study and are thus acknowledged. Appreciation also goes to the external whose clearly detailed and factual publications on assimilation methods made the undertaking more tolerable.

I would also like to extend my gratitude to the teaching staff at the Faculty, specifically ones in the Water Resources scientific research department (WRS), for their dedication and commitment in instilling theoretical as well as practical knowledge on hydrology and remote sensing. I also appreciate the administration for ensuring a seamless study stay. Also grateful to my friends and fellow colleagues for the fun and memorable times we had.

Finally, lots of appreciation to my family; especially me Ma for always being there, *Mungu Akubariki*.

# TABLE OF CONTENTS

---

1.	Introduction.....	1
1.1.	Problem Statement.....	3
1.2.	Research Objectives.....	3
1.3.	Research Questions.....	4
1.4.	Novelty.....	4
2.	Study Area and Materials.....	5
2.1.	Site.....	5
2.2.	Datasets.....	6
3.	Research Theory and Methods.....	9
3.1.	Flow Chart.....	9
3.2.	Soil Moisture Averaging.....	10
3.3.	Effective Measurement Depth.....	12
3.4.	CRP neutron counts correction and smoothing.....	13
3.5.	Neutron counts ( $N$ ) to Soil Water Content.....	14
3.6.	STEMMUS-FT (simulating USWC and SIC).....	14
3.7.	COsmic-ray Soil Moisture Interaction Code (COSMIC).....	15
3.8.	Data Assimilation: Particle Filter.....	16
3.9.	Performance Metrics.....	19
4.	Results and Discussion.....	21
4.1.	CRP Measurements Correction.....	21
4.2.	Nhe COSMIC Tuning.....	22
4.3.	Averaging and No Retrieval.....	22
4.4.	Reference Soil Ice Content.....	26
4.5.	Data Assimilation: Particle Filtering.....	26
4.6.	Limitations.....	44
5.	Conclusion and Recommendations.....	45
5.1.	Conclusion.....	45
5.2.	Recommendations.....	46
6.	List of references.....	47
7.	Appendices.....	52
	Appendix A: Revised weighting parameter functions and constants.....	52
	Appendix B: Smoothing window sensitivity analysis.....	53
	Appendix C: COSMIC states only (and state-parameter) DA experiment flow chart.....	54
	Appendix D: Observed and Simulated ST timeseries and SFCCs.....	55
	Appendix E: Computational demand and smoothness.....	56

# LIST OF FIGURES

---

<b>Figure 1:</b> Maqu SM site, Tibetan Plateau (adapted from data sourced from <a href="http://www.itc.nl">www.itc.nl</a> and <a href="http://gadm.org-via-diva-gis.org">gadm.org-via-diva-gis.org</a> ) .....	5
<b>Figure 2:</b> Neutron counts and soil water content timeseries .....	6
<b>Figure 3:</b> Flow chart of this study .....	9
<b>Figure 4:</b> Data Assimilation Scheme (Particle Filter flow diagram).....	19
Figure 5: Corrected counts, air pressure timeseries. ....	22
<b>Figure 6:</b> Taylor diagram showing comparison of COSMIC derived SWCs with those from equal, conventional and revised weighting approaches over the August to October, 2016 period. ....	23
<b>Figure 7:</b> Cumulative weights over depth (uniform vs conventional vs COSMIC) [Observed SWC-11·10·2016 23:45].....	24
<b>Figure 8:</b> Surface plot showing the CFoC over depth for different SWC averages.....	24
<b>Figure 9: a)</b> Neutron counts, SWC timeseries; <b>b)</b> bias, mean bias (ME) for the different weighting methods.....	25
<b>Figure 10:</b> SIC 'truth' timeseries as well as the average TSWC inferred from CRP corrected counts and average USWC derived by averaging in-situ SM probe observations using the conventional non-linear weighting method.....	26
<b>Figure 11: a)</b> State & state-parameter updates versus open loop (without DA) over the Aug-Oct 2016 period; <b>b)</b> zooming in to the first week of the data series.....	27
<b>Figure 12:</b> Histograms for the last timestep: <b>a)</b> states update only and <b>b)</b> states-Nhe parameter update...28	
<b>Figure 13:</b> Evolution of the site-specific high-energy calibration parameter (Nhe).....	29
<b>Figure 14:</b> False Nhe initialization <b>a)</b> 50 and <b>b)</b> 1500 and the corresponding neutron counts timeseries..29	
<b>Figure 15:</b> Average USWC applying the conventional non-linear method (average for the CRP footprint). .....	31
<b>Figure 16:</b> Scatter diagram showing the simulated against observed USWC (averaged using the conventional non-linear method). ....	32
<b>Figure 17:</b> Observed and simulated freezing-fronts: reproduced from Yu et al. (2018). ....	33
<b>Figure 18:</b> Example illustrating the application of the $0.05m3m - 3$ uncertainty range global perturbation together with histograms for prior ensembles generated for the 5 cm, 40 cm and 80 cm layers (last simulation timestep).....	34
<b>Figure 19:</b> Data Assimilation Scheme (Particle Filter flow diagram) utilizing a pre-compiled look-up table. ....	35
<b>Figure 20:</b> Neutron counts timeseries: simulated open loop (OL), after the implementation of SIR_PF (with $\pm 0.1m3m - 3$ and $\pm 0.05m3m - 3$ uncertainty ranges) and observed. ....	35
<b>Figure 21:</b> Average TSWC timeseries' (reference, OL and analyses).....	36
<b>Figure 22:</b> Scatter plots of simulated neutron counts and average TSWC against their respective reference (observed) states. ....	37
<b>Figure 23:</b> Posterior, prior and likelihood histograms for the last timestep: <b>a)</b> $\pm 0.05m3m - 3$ and <b>b)</b> $\pm 0.1m3m - 3$ uncertainty ranges.....	38
<b>Figure 24:</b> Average SIC timeseries (reference, OL and analyses) and respective scatterplots.....	39
<b>Figure 25:</b> TSWC, USWC and SIC over 5, 10, 20, 40 and 80 cm layers for the different scenarios.....	40
<b>Figure 26: a)</b> Neutron counts timeseries for analysis utilising LUT model generated particles. Analyses from implementations utilizing LUTs with $\pm 0.1$ and $\pm 0.05$ uncertainty ranges added for comparison. Scatter diagrams: <b>b)</b> SFT-OL; <b>c)</b> model LUT (perturbed likelihood/obs.); <b>d)</b> model LUT (unperturbed likelihood/obs.).....	41

<b>Figure 27:</b> Posterior, prior (model simulations LUT; perturbed initial SWC) and likelihood histograms (last timestep). <b>a)</b> perturbed and <b>b)</b> unperturbed likelihood. ....	42
<b>Figure 28:</b> Depiction of the last timestep's TSWC profiles under different scenarios (SFT-OL and analyses) and the prior particles distributions/histograms for the 5, 40 and 80 cm soil layers as compiled from model simulations with perturbed initial soil moisture states. ....	43
<b>Figure 29:</b> Total, frozen and unfrozen average soil water contents. TSWC analysis derived by weighting against unperturbed likelihood in the SIR-PF.....	44
<b>Figure 30:</b> Smoothing window sensitivity analysis based on work by Peng (2017). ....	53
<b>Figure 31:</b> Illustrative COSMIC assimilation experiment.....	54
<b>Figure 32:</b> The observed and simulated ST timeseries' and SFCCs over different layers. ....	55
<b>Figure 33:</b> Computational demand of the SIR-PF utilizing LUTs compiled using $\pm 0.1 \text{ m}^3 \text{ m}^{-3}$ model uncertainty. The LUTs contained 3589 timesteps with varying number of particles. ....	56
<b>Figure 34:</b> Analyses timeseries' obtained from using LUTs (model uncertainty 0.1) with different ensemble members, i.e. from top to bottom: 10, 50, 100, 500, 1000 and 2000 particles, and the corresponding standard deviation of differences (smoothness measure (Hyndman, 2012)). ....	56

## LIST OF TABLES

---

<b>Table 1:</b> CRP data.....	6
<b>Table 2:</b> STEMMUS cardinal input data.....	7
<b>Table 3:</b> COSMIC parameters and input .....	7
<b>Table 4:</b> Simulated-vs-observed states RMSE and Correlation coefficients. ....	32
<b>Table 5:</b> Metrics for open loop and analysis scenarios. ....	37
<b>Table 6:</b> Revised weighting parameter constants. ....	52

## LIST OF ABBREVIATIONS

---

CFoC	Cumulative Fraction of Counts
COSMIC	COsmic-ray Soil Moisture Interaction Code
CRP	Cosmic Ray Neutron Probe
DA	Data Assimilation
EnKF	Ensemble Kalman Filter
FT	Freezing Thawing
LSM	Land Surface Model
MCNPX	Monte Carlo N-Particle eXtensible transport code
SFCC	Soil Freezing Characteristic Curve
SIC	Soil Ice Content
SIR-PF	Sequential Importance Resampling-Particle Filter
ST	Soil Temperature
STEMMUS	Simultaneous Transfer of Energy Mass and Momentum in Unsaturated Soil
SWC/SM	Soil Water Content/Soil Moisture
TSWC	Total Soil Water Content
USWC/LSWC	Unfrozen/Liquid Soil Water Content



# 1. INTRODUCTION

Soil moisture (SM) is a key component in the hydrological cycle that controls the land-atmosphere water and energy interactions (Lakshmi, 2014). Accurate estimation of SM is therefore essential for effective and timely decision making in different hydrological applications such as irrigation scheduling, rainfall-runoff modelling, flood prediction, weather forecasting and freeze-thaw (FT) detection in frozen ground.

SM data has traditionally been collected from in-situ point (sensor) measurements that have an inherent spatial coverage limitation with the classic gravimetric (oven-drying) method commonly being used in their calibration and validation. While remote sensing SM retrievals are able to address the coverage problem, these coarse-scale products are unable to provide accurate estimates at finer scales as has been shown in results by Famiglietti et al. (2008), i.e. SM variability typically increases with extent scale. To bridge this gap, the promising cosmic-ray neutron probe (CRP), which has low dependence on soil type (Zreda et al., 2008), has been used to provide field-scale SM information averaged over several hectares in areal footprint and tens of decimetres in depth profiles (Schrön et al., 2017).

The CRP observation method is based on the principle of neutron thermalization. Hydrogen, which is present in soil water, is the most dominant element in the moderation (thermalization) of fast neutrons (Zreda et al., 2012). Correction for influences on the neutron signal due to changes in air pressure, air humidity and incoming cosmic radiation is needed to ensure reliable inference of total soil water content (TSWC) from measured neutron counts. The most widely applied (Schreiner-McGraw et al., 2016; Schrön et al., 2017; Zreda et al., 2012) counts-to-TSWC translation model is the shape-defining function proposed by Desilets et al. (2010). It is imperative to have the site-specific parameter ( $N_0$ ) accurately calibrated to ensure SM estimates inferred from the neutron counts reflect the available ('true') soil water content. To this end, different SM averaging methods, which take into account the probe's effective measuring depth i.e. the conventional (Franz et al., 2012) and revised (Schrön et al., 2017) weighting approaches, have been proposed for calibration of the CRP. These weighting methods, unlike the uniform (equal) averaging approach, are based on the cosmic neutron creation and transport theory.

Neutron-moderating TSWC in frozen soils exists in ice, liquid and vapor forms. To partition the TSWC, researchers commonly utilize soil freezing characteristic curves (SFCC) that relate the volumetric content of unfrozen (liquid) water to the Soil Temperature (ST) (Koopmans & Miller, 1966; Inaba, 1983; Yu et al., 2018). The quantification and correlation of the unfrozen water and Soil Ice Content (SIC) as functions of ST for studying and modelling the freeze-thaw (FT) process in cold regions is crucial for engineering applications, e.g. design of buried pipelines and petroleum reservoirs, where FT needs to be considered in order to mitigate against possible disasters (Civan, 2000).

To allow the prediction of FT, soil ice content needs to be simulated and this requires estimation of SM and ST states in mass and energy models. In their review, Li et al. (2010) show that models used for prediction of FT in frozen soils vary in their model structure (governing equations) complexities and/or processes considered. Traditional coupled water and energy models used for simulating states in the unsaturated zone are based on the theory by Philip and de Vries (PdV) which disregards flow of the gas phase (Zeng et al., 2011b). The gaseous phase (water vapor and dry air) has been shown to substantially retard or increase the rate of infiltration in some situations, leading to the development of multi-phase models such as STEMMUS, a coupled heat and mass two-phase Land Surface Model (LSM) that simulates states (SM and ST) in the vadose zone (Zeng et al., 2011a). Yu et al. (2018) investigated the STEMMUS-FT model's capacity to simulate simultaneous mass and heat flow in frozen soils. In Maqu, the FT process is characterized by; a freezing period where ST falls from the surface downwards, followed by a transition period where the soil starts getting warmer leading to stability of the ST and finally the thawing period where ST goes above the freezing temperature initiating the thawing front from the topsoil (Yu et al., 2018).

Modelled SM data are likely to deviate from measurements due to systematic bias resulting from errors in the forcing information, model structure, parameters as well as uncertainties in observed data as described by instrument errors. To address such uncertainties, data assimilation (*also* inverse modelling) of soil moisture observations to update model simulations has been applied in past studies. Data assimilation (DA) is the integration of near real-time observations (likelihood function) with the numerical model output data (prior distribution) to give enhanced estimates (posterior distributions) of the evolving system states (Swinbank & O'Neill, 1994). Assimilation studies utilize measured and remotely sensed data with different ensemble based DA algorithms, e.g. the Ensemble Kalman Filter (EnKF), Particle Filter (PF) or variational methods (3/4D VAR), being applied in majority of the studies, *viz.*, joint state-parameter estimation (Han et al., 2015; Montzka et al., 2011; Moradkhani et al., 2005) and updating of states in a (calibrated) model (Draper et al., 2011; Shuttleworth et al., 2013).

Monte Carlo based simulations, under which the PF particularly falls, have not been spared from criticism. In their discussion, Beisbart et al. (2013) claimed that Monte Carlo methods provide limited source of knowledge on physical processes under investigation terming them “merely elaborate arguments”. Nonetheless, it has been shown in several reviews (Evensen, 2003; Keller et al., 2018; Montzka et al., 2012; Moradkhani, 2008; Ngodock et al., 2006; Pauwels & Lannoy, 2009; Zhang et al., 2017) that by combining these methods with theoretical knowledge of the physical system, i.e. models, better predictions of the evolving states can be achieved; this is especially true for environmental processes which exhibit random walks/variability over space and time.

By translating modelled SM estimates to neutron counts, CRP field observations can be used as likelihood in DA schemes to correct for systematic LSM biases and thus improve the estimates. Algorithms that derive counts from SM simulations include the Monte Carlo N-Particle eXtended (MCNPX) neutron transport

code and the Cosmic-ray Soil Moisture Interaction Code (*COSMIC*) (Shuttleworth et al., 2013). Both codes are accurate but *COSMIC* is preferred for practical assimilation applications as it computes at an infinitesimal fraction of the time taken by *MCNPX* i.e. it is 50000 times faster than *MCNPX* (Shuttleworth et al., 2013). In calculating the counts from a given SM profile, *COSMIC* assumes the existence of three dominant processes in the generation of fast neutrons, namely: exponential reduction of high energy neutrons with depth; fast neutrons creation at all depths depending on number of high energy neutrons, density of dry soil and density of soil water per unit soil volume; and the proportion of fast-neutrons detected above the ground is attenuated exponentially by a factor related to the distance between origin of the neutrons and the detector (Shuttleworth et al., 2013).

In this study, assimilation of observed cosmic-ray neutron counts using a particle filtering framework that combines *STEMMUS* and *COSMIC* was done to reduce the deviation of simulated estimates from observed measurements. The selection of the multi-phase *STEMMUS* for this study is supported by the finding that in frozen soils, vapor instead of liquid flow contributes most to the total mass flux because of the ice blocking effect (Yu et al., 2018).

### **1.1. Problem Statement**

Soil Ice Content is difficult to measure using traditional methods. The classical oven drying method, for example, can only quantify the TSWC as soil ice will be liquified once soil temperatures go above zero Celsius. The use of point SM sensors, apart from having limited spatial coverage, requires complicated procedures to partition between unfrozen and frozen water content. The current strategy for obtaining SIC in frozen soils is through the determination of USWC and TSWC. The assumption that the USWC-relative dielectric permittivity (USWC- $\epsilon_r$ ) relationship in frozen soils is similar to that for un-frozen soils (Patterson & Smith, 1981) makes derivation of the USWC from field observations practically possible. Measurement of TSWC, however, needs dedicated geophysical approaches, for example, using Nuclear Magnetic Resonance (NMR) or Gamma Ray Attenuation methods. As an alternative, the cosmic-ray probe (CRP) provides an effective and reasonable means for monitoring the TSWC.

### **1.2. Research Objectives**

The main objective of this research is to improve the determination of SIC by assimilating CRP observations into the *COSMIC* model by sequentially integrating the soil states required for calculation of neutron counts from *STEMMUS* simulations.

Specific objectives;

- Correction and smoothing of the CRP neutron measurements over the Maqu site before use as reference.

- Calibrate the site-specific parameter  $N_0$  using different weighting/averaging methods. For comparison with  $N_0$  obtained from the use of uniform weighting.
- Forward simulation of fast-neutron counts by coupling STEMMUS and the COSMIC code.
- Sequentially assimilate the CRP neutron measurements to update STEMMUS SM states using COSMIC as the observation operator.

### 1.3. Research Questions

To achieve the defined objectives, the following research questions are highlighted;

- Is the use of uniform weighting method for calibrating the CRP theoretically founded?
- Is it beneficial to assimilate CRP measurements to update STEMMUS simulations for Maqu?
- Can the heat exchanges in STEMMUS be used to quantify SIC and thus detect the freezing-thawing process in Maqu?
- How well the approach proposed in this study can capture the observed (CRP's TSWC—probe's USWC) SIC in Maqu and why?

### 1.4. Novelty

- The CRP measurements, combined with in-situ ST and the Soil Freezing Characteristic Curve, will be used to quantify SIC.
- Furthermore, the process model, STEMMUS, will be coupled with the observation model, COSMIC, to develop a forward signal simulator for neutron counts for onward utilization in a PF DA framework.

## 2. STUDY AREA AND MATERIALS

### 2.1. Site

This study was carried out in the Maqu site which is situated in the expansive Tibetan Plateau ( $33^{\circ} 30' - 34^{\circ} 15' \text{ N}$ ,  $101^{\circ} 38' - 102^{\circ} 45' \text{ E}$ ) with elevations upwards of 3200 m a.s.l. The area experiences dry winters (coldest month: January) and rainy summers (warmest month: July) with the annual mean air temperature being  $1.28^{\circ} \text{ C}$  (Yu et al., 2018). These low temperatures, coupled with the site's frost-susceptible silty-loam soil type, make FT processes common during winter. The site is equipped with: an automatic soil moisture soil temperature (SMST) monitoring network (ECH20 probes) sensing at 5cm, 10cm, 20cm, 40cm, 80cm and 160cm depths; a cosmic-ray probe (CRP); a 20m Planetary Boundary Layer (PBL) tower that provides wind speed, air humidity and temperature observations at five above-ground heights; and an eddy-covariance (EC) system (Dente et al, 2012).

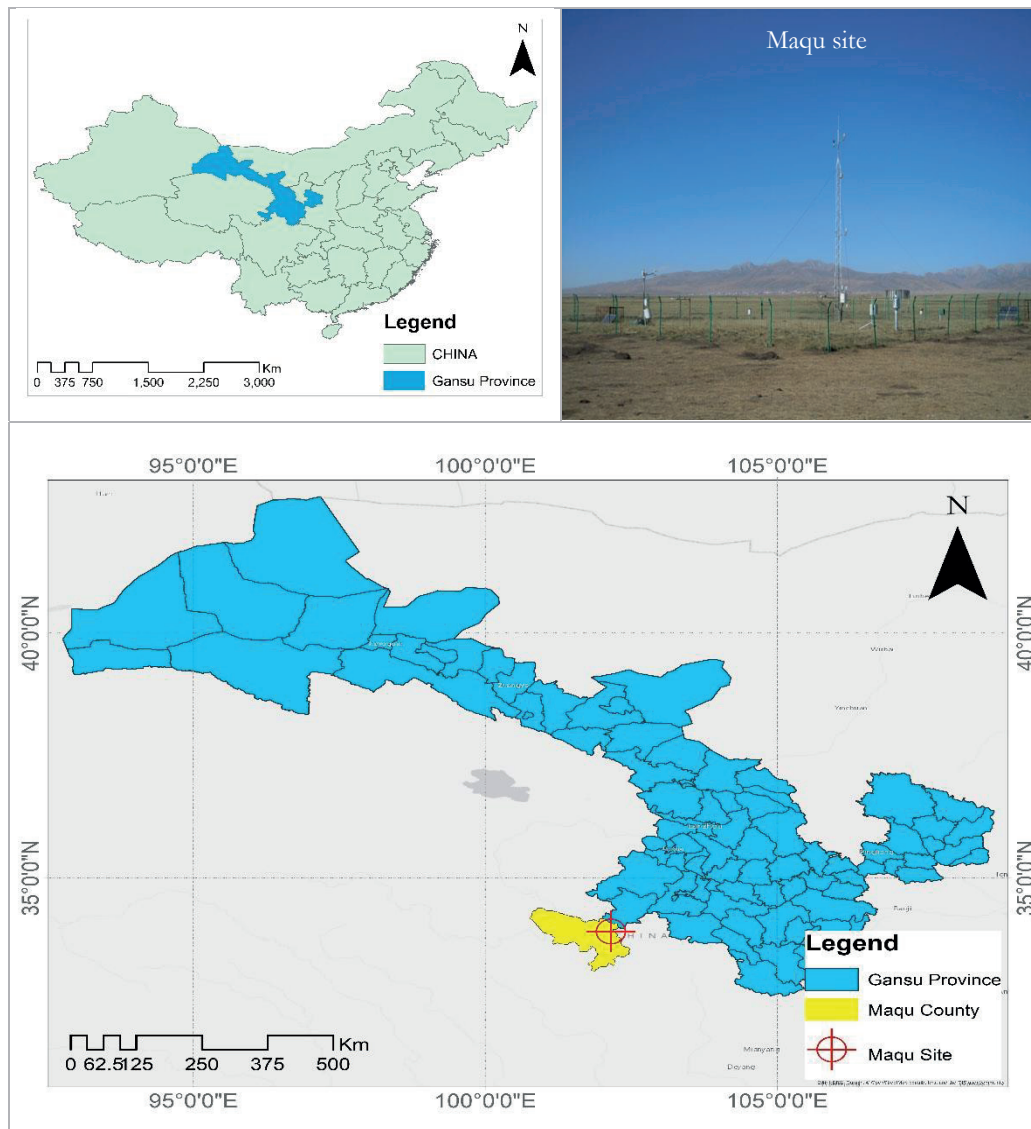


Figure 1: Maqu SM site, Tibetan Plateau (adapted from data sourced from [www.itc.nl](http://www.itc.nl) and [gadm.org-via-diva-gis.org](http://gadm.org-via-diva-gis.org))

## 2.2. Datasets

The data utilized for this study is divided into three i.e. cosmic-ray neutron probe (CRP) data, input data for the STEMMUS model and data related to the COSMIC code. Output from the processes also served as input into other processes as is presented in the flow diagram (Figure 3). The datasets used are listed below;

### 2.2.1. Cosmic Ray Neutron Probe (CRP)

The CRP provides the above ground neutron counts which need to be corrected for air relative humidity, pressure and incoming cosmic-ray flux. These data are collected simultaneously by the probe after every fifteen minutes allowing correction of the moderated counts and inference of TSWC.

**Table 1:** CRP data.

Type of data	unit
• Cosmic Ray Probe neutron counts (N)	[counts/h]
• Site specific calibration parameter (N <sub>0</sub> )	[counts/h]
• Air pressure	[hPa]
• Air relative humidity	[%]

Figure 2 below shows a sample time series (May 2016) of CRP counts and averaged SM for Maqu site upon which Peng's (2017) sensitivity analysis (Appendix B) was based;

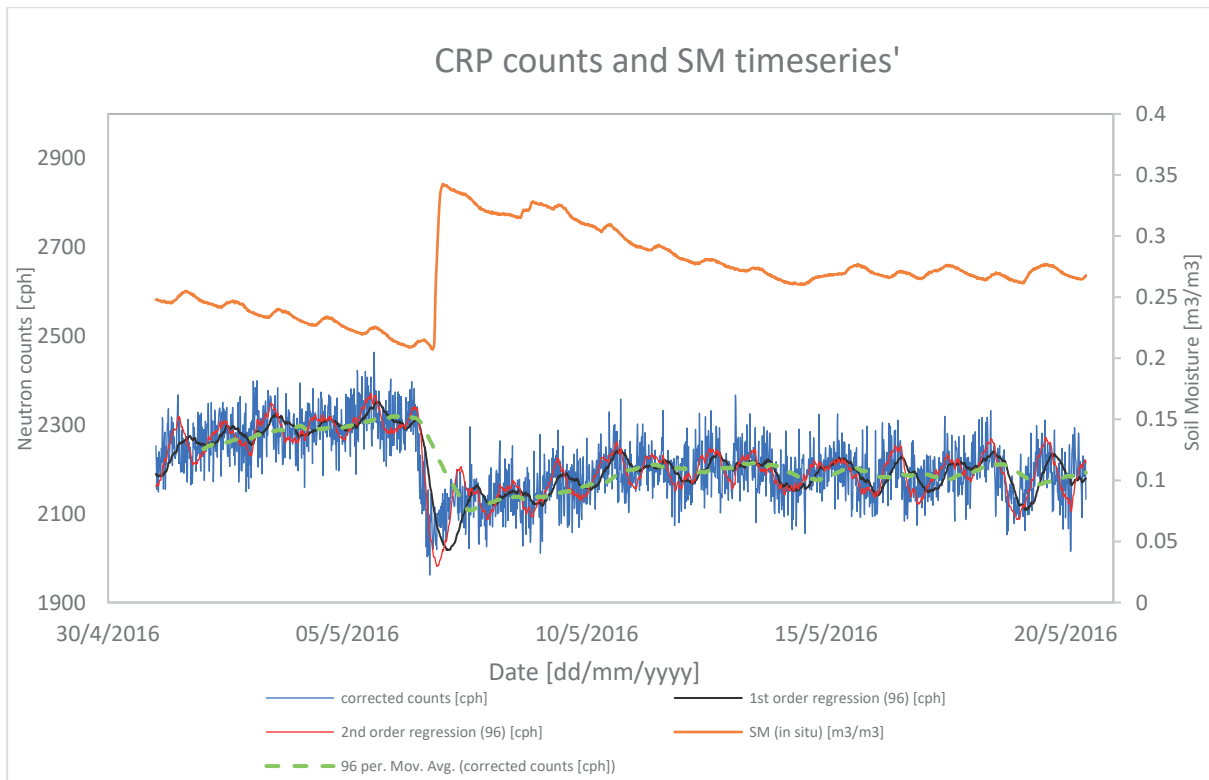


**Figure 2:** Neutron counts and soil water content timeseries

This cosmic neutron data, in addition to being the proxy from which reference TSWC was derived, served as the likelihood used in data assimilation scheme setups.

### 2.2.2. STEMMUS

The STEMMUS land surface model provides estimates for different user-defined soil layers covering the surface and root zone i.e. at depths ranging from 0.1 cm to 160 cm. To simulate the states, STEMMUS requires as inputs: forcing data, initial state conditions, boundary conditions and system parameters. The key inputs are tabulated in [Table 2](#);

**Table 2:** STEMMUS cardinal input data

Type of data	unit
• Precipitation	[mm]
• Air temperature	[°C]
• Air relative humidity	[%]
• Wind speed	[m/s]
• Surface temperature	[°C]
• Atmospheric pressure	[hPa]
• Initial SWC	$[m^3/m^3]$
• Initial ST	[°C]
• Saturated Hydraulic Conductivity (K)	[m/s]
• Porosity	$[m^3/m^3]$
• Saturated and residual SWC	$[m^3/m^3]$
• van Genuchten parameters; $\alpha$	$[cm^{-1}]$
$n$	[-]

### 2.2.3. COSMIC

COSMIC is a neutron-count forward simulation model that calculates equivalent neutron counts from soil moisture (measured and/or simulated). [Table 3](#) summarises the data required as input for the model.

**Table 3:** COSMIC parameters and input

Type of data	unit
• High energy and fast neutron soil and water attenuation lengths, L1, L2, L3 & L4	$[g/cm^2]$
• Dry soil bulk density ( $\rho_s$ ) and total soil water density ( $\rho_w$ )	$[g/cm^3]$
• High energy neutron creation parameter (N)	[-]
• SWC estimates from STEMMUS (in-situ SWC measurements are used in the model's calibration)	$[m^3/m^3]$

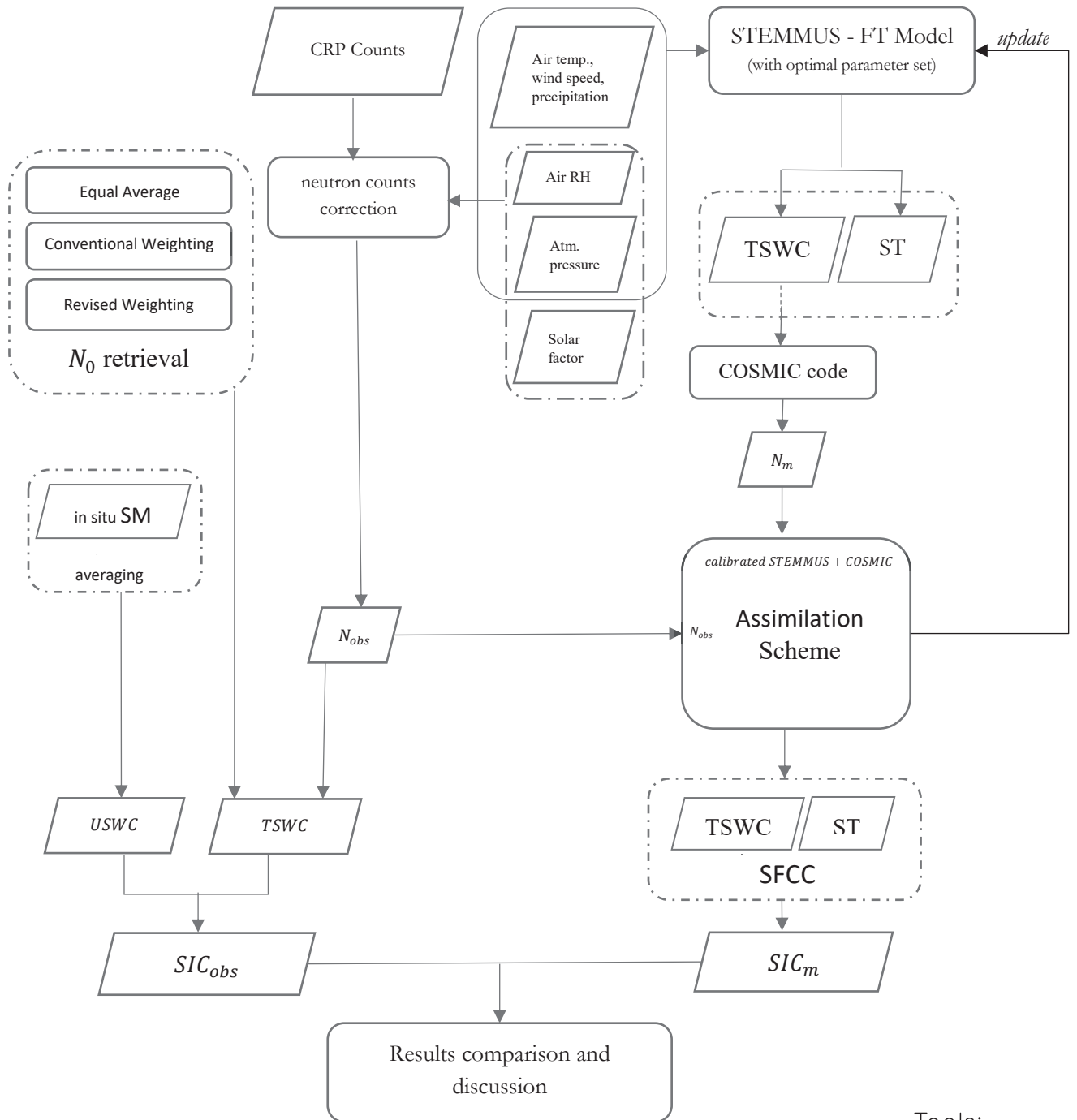
#### **2.2.4. SMST Network Data**

As pointed out earlier, Maqu site is instrumented with soil moisture and soil temperature sensors. These were treated as the sources of reference SM and ST data against which simulated states were validated. During the winter season, measurements from in-situ SM probes were taken to represent the ‘true’ USWC.

### 3. RESEARCH THEORY AND METHODS

#### 3.1. Flow Chart

The flow diagram below summarises the methods as applied in this study;



Tools:  
 - MATLAB®  
 - Excel®

Figure 3: Flow chart of this study.

### 3.1.1. Summary of Data Analysis Methods

To achieve the objectives of this research, a methodical approach as summarized below and illustrated in the flowchart ([Figure 3](#)) was implemented.

The moderated neutron counts as observed by the CRP were first corrected for atmospheric pressure, air humidity and incoming cosmic-rays effects. The corrected counts were then subjected to a *Savitzky-Golay* least squares smoothing filter to reduce the sharp and abrupt variations over time.

The conventional (both linear and non-linear vertical) and revised weighting methods were then implemented for comparison with the equally weighted approach. The sampling soil water dataset as collected by Peng, (2017) was averaged using the different methods and used to derive the site-specific calibration parameter ( $N_0$ ). Selection of the most ideal (for this study) weighting method was based on comparison with COSMIC derivations.

With the calibrated  $N_0$ , the average reference TSWC was derived and by using the selected weighting method, the USWCs as observed by in-situ probes could hence be averaged. The reference SIC was consequently computed to serve later as the ‘truth’ upon which the simulated SICs were validated.

The process model (STEMMUS-FT) was then set up for several experiments. The model as calibrated in Yu et al. (2018) was run and the simulated states (Open Loop simulation results) used in further data assimilation scenarios. A sequential importance resampling PF assimilation framework, which incorporated simulated states and the observation model (COSMIC), was developed for updating the modelled TSWC and thus correcting the forecasted SIC.

Subsequent sections in this chapter expound on the research methodology as considered and implemented in this study.

## 3.2. Soil Moisture Averaging

Different methods have been used to calibrate and validate the CRP i.e. equal average, conventional and revised weighting approaches. Since different points in the CRP’s footprint contribute differently to the measured signal counts depending on the distance from the probe and depth of the soil layer, different weights need to be assigned (Schrön et al., 2017). The equally weighting method has thus been replaced with the conventional and revised methods in current CRP calibration/validation campaigns.

### 3.2.1. Equal Average Weighting

The general averaging equation as given below is applied;

$$\theta_{ave} = \frac{\sum_{i=1}^n w_i \theta_i}{\sum_{i=1}^n w_i} \quad (1)$$

where  $\theta_i [m^3m^{-3}]$  is the SWC at layer  $i$  for a given profile,  $n$  is the combined number of layers in all soil sampling profiles and  $w_i$  is the weight assigned to layer  $i$  ( $w_i$  is equivalent to  $1/n$  in the equally weighted approach).

### 3.2.2. Conventional Weighting

Based on the weighting functions from Franz et al. (2012). The averaging iteration is implemented using Equations (2) and (3) until convergence to a user defined range is attained. The weights for the sampling layers and profiles are assigned based on the depth from the surface and distance from the CRP respectively.

$$w_d^{conv} = \begin{cases} 1 - d/D^{conv}, & d \leq D^{conv} \\ 0, & d > D^{conv} \end{cases} \quad (2)$$

$$w_r^{conv} = \begin{cases} e^{-r/127}, & r \leq 300 \text{ m} \\ w_{r=300}^{conv}, & r > 300 \text{ m} \end{cases} \quad (3)$$

where  $w_d^{conv} [-]$  is the vertical weight for each layer at depth  $d[\text{cm}]$  in a profile,  $D^{conv} = z^*[\text{cm}]$  is the effective measurement depth of the CRP derived using Equation (9),  $w_r^{conv}$  the horizontal weight for each profile and  $r [\text{m}]$  is the distance from the sampling profile to the CRP probe.

On the other hand, the non-linear conventional method, as proposed in Bogena et al. (2013), computes the Cumulative Fraction of Counts (CFoC) over the vertical profile non-linearly and ensures that some weights are assigned to layers below the effective depth  $z^*$  with the bottom getting the residual. Equation (2) thus transforms to;

$$w_d^i = \begin{cases} CFoC_1, & \text{for top soil layer } i = 1 \\ CFoC_i - CFoC_{i-1}, & \text{for other layers; from } i = 2, \dots, b - 1 \\ 1 - \sum_{i=1}^{b-1} w_d^i, & \text{for the bottommost layer } b \end{cases} \quad (4)$$

where  $CFoC$  is the Cumulative Fraction of Counts for the  $i^{\text{th}}$  layer at depth  $d_i$  given by;

$$CFoC_i = 1 - e^{-d_i/\gamma} \quad (5)$$

$$\gamma = \frac{-5.8}{\ln(0.14) \times (H_p + 0.0829)} \quad (6)$$

$H_p$  is the hydrogen pool present in the soil profile i.e. soil moisture, lattice water, soil organic water.

### 3.2.3. Revised Weighting

The conventional method assumes similar penetration depths of detected counts for all distances  $r$  from the sensor. To address this shortcoming, Schrön et al. (2017) proposed the revised averaging approach. Similar to the conventional approach, the averaging is implemented iteratively until the predefined convergence criteria is fulfilled.

$$w_d = e^{-2d/D_p} \quad (7)$$

$$w_r = \begin{cases} (F_1 e^{-F_2 r^*} + F_3 e^{-F_4 r^*})(1 - e^{-F_0 r^*}), & 0m < r \leq 1m \\ F_1 e^{-F_2 r^*} + F_3 e^{-F_4 r^*}, & 1m < r \leq 50m \\ F_5 e^{-F_6 r^*} + F_7 e^{-F_8 r^*}, & 50m < r < 600m \end{cases} \quad (8)$$

where  $w_d$  [-] is the layer vertical weight;  $D_p [cm] = \frac{1}{\rho_{bd}} \left( p_0 + p_1 (p_2 + e^{-p_3 r^*}) \frac{p_4 + \theta}{p_5 + \theta} \right)$  is the revised penetration depth which varies slightly from the effective measurement depth ( $z^*$ );  $p_i$  are horizontal weighting parameters as given in Schrön et al. (2017);  $F_i$  are parameter functions as given in Schrön et al. (2017);  $r^*$  [m] is the rescaled distance ( $r$  as a function of air pressure, vegetation height and SWC). [Appendix A](#) lists the  $p_i$  (parameter constants - [Table 6](#)) and  $F_i$  (parameter functions).

The revised and conventional (linear and non-linear vertical) weighting iteration steps are summarised below (*for more details please see Schrön et al. (2017)*):

1. Estimate initial value (taken as the equally weighted average over all profiles and layers ( $\theta$ )).
2. Calculate the penetration depth for each profile ( $D^{\text{conv}}$  or  $D_p$ )
3. Derive weighted average for each profile ( $\theta_p$ ) by vertically averaging the layers' SWC values.
4. Weight the profiles ( $\theta_p$ ) for derivation of the horizontal footprint average ( $\theta$ ).
5. With the new  $\theta$ , repeat 1-5 until convergence to within the user-defined criteria (1e-6 in this study) is attained.

### 3.3. Effective Measurement Depth

The effective measurement depth, which ranges from 0.12 m (wet soils) to 0.76 m (dry soils), is the soil column where 86% ( $1 - 1/e^2$ ) of the fast neutrons that reach the probe originate (Zreda et al., 2008).

Franz et al. (2012) developed a function for the derivation of the sensor's effective depth ( $z^*$ );

$$z^* = \frac{5.8}{\frac{\rho_{bd}}{\rho_w} (\tau + soc) + \theta + 0.0829} \quad (9)$$

where 5.8 [cm] is the sensitivity depth for 86% of cumulative fast neutrons in liquid water,  $\rho_{bd}$  [ $g\ cm^{-3}$ ] is the soil bulk density,  $\rho_w$  [ $g\ cm^{-3}$ ] is the water density assumed to be  $1\ g\ cm^{-3}$ ,  $\tau$  the weight fraction of lattice water and  $soc$  [ $g\ g^{-1}$ ] the soil organic water content.

### 3.4. CRP neutron counts correction and smoothing

The moderated neutron counts measured by the probe need to be corrected for differences in atmospheric relative humidity, atmospheric pressure and variations in incoming cosmic-ray flux. The different correction factors can be derived using standard approaches (Hawdon et al., 2014; Rosolem et al., 2013; M. Zreda et al., 2012) and correction done as follows;

$$N_{corr} = N_{mod} \times f_{wv} \times f_p \times f_i \quad (10)$$

where  $N_{corr}$  [counts  $hr^{-1}$ ][cph] is the corrected counts,  $N_{mod}$  [cph] is the moderated counts measured by the probe,  $f_{RH}$  [-] is the relative humidity variation correction factor,  $f_p$  [-] is the atmospheric pressure variation correction factor and  $f_i$  [-] is the incoming cosmic-ray correction factor. The formulas to compute the correction factors are as under;

$$f_{wv} = 1 + 0.0054(\rho_{v0} - \rho_{v0}^{ref}) \quad (11)$$

where  $\rho_{v0}$  [ $g\ m^{-3}$ ] is the absolute humidity and  $\rho_{v0}^{ref}$  [ $g\ m^{-3}$ ], the reference absolute humidity.

$$f_p = \exp\left[\frac{P - P_0}{L}\right] \quad (12)$$

$P$  [hPa] is the measured air pressure,  $P_0$  [hpa] is the reference atmospheric pressure, and  $L$  [ $g\ cm^{-2}$ ] is the mass attenuation length for high energy neutrons (value varies between  $\sim 128\ g\ cm^{-2}$  and  $\sim 142\ g\ cm^{-2}$  at high latitudes and the equator respectively (M. Zreda et al., 2012)).

$$f_i = \frac{I_{ref}}{I} \quad (13)$$

$I$  is the selected neutron monitor counting rate at any time while  $I_{ref}$  is a reference counting rate for the same monitor at a fixed time.

Observed CRP neutron counts exhibit large fluctuations over time and therefore need smoothing for better comparability to the soil moisture variations. The *Savitzky-Golay* filter, which is based on the Least Squares Method, was preferred as it is able to extract as much information as is possible (Savitzky & Golay, 1964).

### 3.5. Neutron counts ( $N$ ) to Soil Water Content

The shape-defining function derived by Desilets et al. (2010) after fitting observed SWC with ground-level neutron counts simulated in MCNPX was used to derive the average TSWC.

$$\theta(N) = \frac{a_0}{\left(\frac{N}{N_0}\right) - a_1} - a_2 \quad (14)$$

where  $\theta$  [ $m^3m^{-3}$ ] denotes the volumetric SWC after accounting for the soil bulk density,  $a_0 = 0.0808$ ,  $a_1 = 0.372$  &  $a_2 = 0.115$  are the SWC dependence of near-surface intensity parameters,  $N$  [cph] are the corrected neutron counts and  $N_0$  [cph] is the site specific calibration parameter.

### 3.6. STEMMUS-FT (simulating USWC and SIC)

The STEMMUS model can simulate the unfrozen soil water content (USWC) by exploiting the relation between liquid water and ST as is described by the soil freezing characteristic curve (SFCC). After quantification of USWC, the TSWC can thus be partitioned into USWC and SIC. The multi-phase heat and mass theoretical aspects of STEMMUS are extensively elaborated in Zeng (2013) and Yu et al. (2018).

#### 3.6.1. TSWC from the SWRC

STEMMUS-FT numerically solves for the TSWC by implementing a van Genuchten based Soil Water Retention Curve (SWRC) as given by Equation (15);

$$\theta_{tswc}(h) = \begin{cases} \theta_r + \frac{\theta_s - \theta_r}{[1 + |\alpha h|^n]^m}, & h < 0 \\ \theta_s, & h \geq 0 \end{cases} \quad (15)$$

where  $\theta_{tswc}$  is the total soil water content,  $\theta_s$  &  $\theta_r$  are the saturated and residual water contents respectively,  $\alpha$  is a factor related to the inverse air-entry pressure,  $h$  is the pre-freezing soil potential and  $n$  &  $m = 1 - 1/n$  are empirical shape parameters related to the pore size distribution. For Maqu, Zhao et al. (2018) recommend the pedotransfer functions (PTFs) by Wösten et al. (1999) for fitting the van-Genuchten parameters,  $\alpha$  and  $n$ .

#### 3.6.2. Derivation of USWC using SFCC

Yu et al. (2018) implemented two different SFCC expressions in STEMMUS-FT to quantify the USWC, i.e.;

1. Clapeyron and van Genuchten model

$$\theta_L(h, T) = \theta_r + \frac{\theta_s - \theta_r}{[1 + |\alpha(h + h_{Frz})|^n]^m} \quad (16)$$

where  $\theta_L$  is the liquid/unfrozen soil water content;  $\theta_s$ ,  $\theta_r$ ,  $\alpha$ ,  $h$ ,  $n$  and  $m$  are as previously defined;  $h_{Frz} = \frac{L_f}{gT_0} (T - T_0) * H(T - T_{CRIT})$  is the freezing soil potential,  $L_f$  is the latent heat of fusion,  $g$  is the gravity acceleration,  $T_0$  (273.15 K) is the absolute temperature,  $T$  the soil temperature and  $T_{CRIT} = T_0 + \frac{ghT_0}{L_f}$  is the soil freezing temperature with  $H(\cdot)$  being the Heaviside step function.

## 2. Clapeyron and Clapp & Hornberger model

$$\theta_L(h, T) = \theta_s \left( \frac{L_f}{g\psi_s} \frac{T - T_f}{T} \right)^{-1/b} \quad (17)$$

where  $L_f$  is the latent heat of fusion,  $T$  the soil temperature,  $\psi_s$  the air-entry pore water potential and  $b$  is the empirical Clapp-Hornberger parameter.

### 3.6.3. Soil Ice Content (SIC)

The total water conservation equation for the derivation of SIC is given below;

$$\theta_{tswc} = \theta_{uswc} + \theta_{sic} \quad (18)$$

where  $\theta_{tswc}$ ,  $\theta_{uswc}$  and  $\theta_{sic}$  are the total soil water, unfrozen or liquid soil water and soil ice contents, respectively. Difference in liquid and ice water densities is accounted for in derivation of effective density of the total volumetric soil water content.

### 3.7. COsmic-ray Soil Moisture Interaction Code (COSMIC)

As has been presented, the COSMIC model assumes three dominant processes when calculating neutron counts from soil moisture (Shuttleworth et al., 2013) and is expressed as follows:

$$N_{COSMOS} = N_{he} \int_0^{\infty} \left\{ A(z) [\alpha \rho_s(z) + \rho_w(z)] \exp \left( - \left[ \frac{m_s(z)}{L_1} + \frac{m_w(z)}{L_2} \right] \right) \right\} dz \quad (19)$$

where

- $N_{he}$  is the high energy neutron flux given by  $CN_{he}^0$  ( $C$  – fast neutron creation constant for pure water;  $N_{he}^0$  – number of high-energy neutrons at the soil surface),  $\rho_s(z)$  is the local bulk density of dry soil,  $\rho_w(z)$  the total soil water density,  $L_1 = 161.986 \text{ g cm}^{-2}$  and  $L_2 = 129.146 \text{ g cm}^{-2}$  are the high energy soil and water attenuation lengths respectively,  $m_s(z)$  and  $m_w(z)$  are the integrated mass per unit area of dry soil and water respectively.

- $A(z)$  – integrated average attenuation of the neutrons generated at depth  $z$  given by;

$$A(z) = \left(\frac{2}{\pi}\right) \int_0^{\pi/2} \exp\left(\frac{-1}{\cos(\theta)} \left[\frac{m_s(z)}{L_3} + \frac{m_w(z)}{L_4}\right]\right) d\theta \quad (20)$$

where  $\theta$  is the angle between the vertical below the detector and the line between the detector and each point in the plane,  $L_3$  and  $L_4 = 3.163 \text{ g cm}^{-2}$  are the fast neutron soil and water attenuation lengths.  $L_3$  can be correlated to  $\rho_s$  and a regression similar to Equation (21) fitted;

$$L_3 = -31.65 + 99.29\rho_s \quad (21)$$

- $\alpha$  is the relative (soil vs water) fast neutron efficiency of creation factor given by;

$$\alpha = 0.404 - 0.101\rho_s \quad (22)$$

During winter periods, calculation of  $m_w$  should consider both the densities of frozen and un-frozen phases of water. In light of this, minor modifications were made to the COSMIC code to account for the effective density of water;

$$\rho_{eff} = f_{uswc} \times \rho_{uswc} + f_{ice} \times \rho_{ice} \quad (23)$$

$$m_w = \rho_{eff} \times TSWC \quad (24)$$

where  $\rho_{eff}$  is the water effective density,  $f_{uswc}$  and  $f_{ice}$  are the liquid and water fractions respectively,  $\rho_{uswc}$  and  $\rho_{ice}$  are the liquid and ice densities respectively,  $TSWC$  is the volumetric total soil water and  $m_w$  the integrated water mass per unit area for a unit depth as used in Equations (19) and (20).

The  $N_{he}$  parameter should be calibrated before the COSMIC observation model can be used i.e. by tuning it to reproduce CRP fast neutron measurements utilizing soil water content observations as input. Baatz et al. (2014) fitted a linear equation, using 16 calibration datasets, that relates the site-specific calibration parameter ( $N_0$ ) with the high energy neutron flux parameter ( $N_{he}$ ) as given in Equation (25). This linearly fitted regression served as a quick check to ensure the tuned  $N_{he}$  was within the feasible range.

$$N_{he} = 0.1612N_0 + 7.1956 \quad (25)$$

### 3.8. Data Assimilation: Particle Filter

Data assimilation schemes are based on Bayesian inference methods that combine prior information (model forecasts/background) with the likelihood function (observations) to estimate the posterior distribution (the analysis) of model states and/or parameters. Analytical expressions of the posterior distribution can be derived for simple applications but for complex problems, they are approximated recursively often using

either the Kalman Filter (Kalman, 1960) (with its ensemble-based variant, the EnKF (Evensen, 1994), applied in most studies) or the Particle Filter (Sequential Monte Carlo (SMC)) method (Gordon et al., 1993).

The Particle filtering algorithm was preferred in this study as it is able to handle higher statistical moments (mode and kurtosis), in addition to mean and (co-) variance that are tracked in the Ensemble Kalman Filter (EnKF), and thus giving a relatively full representation of the posterior (Moradkhani et al., 2005). Furthermore, unlike the EnKF which requires linearization of the observation operator when calculating the Kalman gain (Montzka et al., 2012), the particle filter allows the use of non-linear observation models in their original form.

### Sequential Importance Resampling Particle Filter (SIR-PF)

Particle filters are sequential Monte Carlo based methods used in estimating the posterior distribution where the Bayesian update step is approximated non-linearly and can therefore handle non-Gaussian distributions effectively (Montzka et al., 2012).

In the PF, each ensemble member (state *(and parameter in the joint state-parameter case)* particle) is propagated forward in time using the process model;

$$x_t^{i-} = f(x_{t-1}^{i+}, \theta, u) + \omega \quad (26)$$

where  $x$  represents the states with  $i$  being the ensemble particle.  $-$  and  $+$  superscripts represent the *a priori* and *a posteriori* estimates respectively. The analysis ensemble from the previous timestep,  $t-1$ , is propagated through the process model,  $f$  (e.g. in this case *STEMMUS-FT*), to obtain the background at time  $t$ . Forcing data ( $u$ ) and model parameter ( $\theta$ ) particles serve as inputs.  $\omega$  is an assumed model error.

An observation model, as given in Equation (27), which relates the modelled states to observations is used to transform the simulations for later approximation of the posterior distribution.

$$y_t = h(x_t^{i-}, \theta) + v \quad (27)$$

where  $y_t$  is the ensemble vector of mapped model states.  $h(\cdot)$  is a non-linear observation operator (in this case *COSMIC*) which maps the modelled state particles,  $x_t^{i-}$ , to variables equivalent to the observed measurements i.e. the CRP neutron counts.  $\theta$  here refer to observation model parameters e.g. the high energy creation parameter (Nhe).  $v$  is an assumed prediction error.

Particle filters estimate the posterior using discrete random particles and their associated weights (Moradkhani et al., 2005).

$$p(x_{1:t} | y_{1:t}) = \sum_{i=1}^N w_t^i \delta(x_{1:t} - x_{1:t}^i) \quad (28)$$

where  $w_t^i$  is the weight of the  $i^{\text{th}}$  particle,  $N$  is the number of ensemble members (particles) and  $\delta(\cdot)$  is the Dirac delta function.

Since the true posterior distribution as given by Bayes' theorem is unknown, deriving particles from it is impractical, making it feasible to draw the particles from an importance (proposal) distribution (Montzka et al., 2012; Moradkhani et al., 2005). Importance weights are expressed as follows;

$$w_t^i \propto w_{t-1}^i \frac{p(y_t | x_t^i) p(x_t^i | x_{t-1}^i)}{q(x_t^i | x_{t-1}^i, y_t)} \quad (29)$$

where  $p(y_t | x_t^i)$  is the likelihood (a Gaussian distribution, as given by Equation (31), is generally assumed for its estimation),  $p(x_t^i | x_{t-1}^i)$  is the transition prior and  $q(x_t^i | x_{t-1}^i, y_t)$ , the proposal distribution. Since it is common to select the transition prior as the proposal distribution (Gordon & Salmond, 1993; Montzka et al., 2012; Moradkhani et al., 2005), Equation (29) reduces to;

$$w_t^i \propto w_{t-1}^i p(y_t | x_t^i) \quad (30)$$

$$p(y_t | x_t^i) \approx L(y_t | x_t^i) = \frac{1}{\sqrt{(2\pi\sigma_{obs}^2)}} e^{-\frac{(y-h(x))^2}{2\sigma_{obs}^2}} \quad (31)$$

In Particle Filters with Sequential Importance Resampling (SIR), only particle weights are updated with the state (*and parameter: in the joint state-parameter assimilation case*) particles being resampled according to their likelihood weights (probabilities), where highly weighted particles are replicated while those with negligible weights are discarded thus avoiding particle degeneration.

Since resampling tends to alter the ensemble's probability density function (pdf) leading to a generally poor representation of the posterior, several authors such as Moradkhani et al. (2012) and Zhang et al. (2017), have proposed the use of a limiting measure (an effective sample size) to identify the degeneracy of particles before the implementation of SIR. The effective sample size ( $N_{eff}$ ) as given by Equation (32) is computed and then compared to a pre-set threshold (usually  $N/2$ ) consequently executing the resampling (SIR) algorithm if the  $N_{eff} < N/2$  condition is met.

$$N_{eff} = \frac{1}{\sum_{i=1}^N (w_t^i)^2} \quad (32)$$

After resampling, all particles are assigned equal weights ( $1/N$ ) and then propagated forward in time through  $f(\cdot)$ . In cases where model parameters are updated i.e. in joint state-parameter assimilation, a minor parameter

perturbation should be carried out to prevent sample impoverishment (Montzka et al., 2011; Moradkhani et al., 2005). [Figure 4](#) summarizes the standardized fully coupled SIR-PF framework.

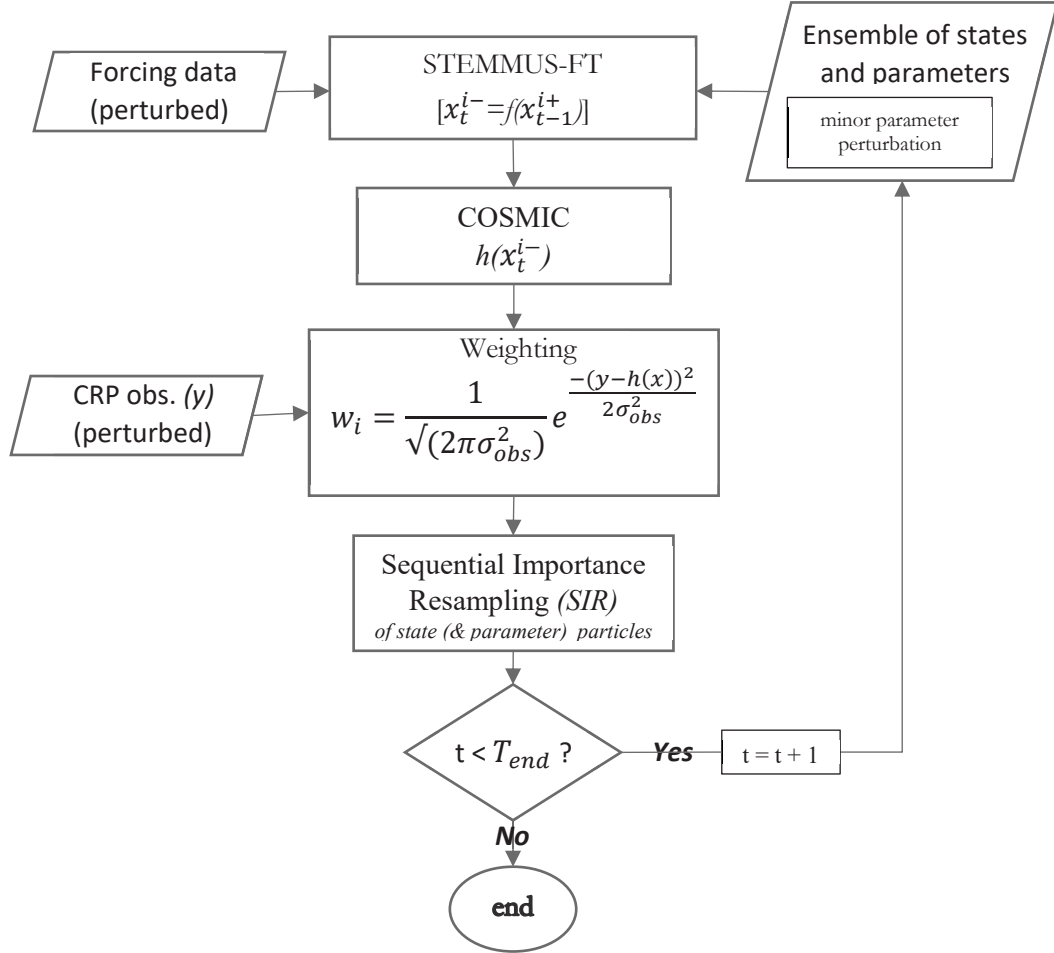


**Figure 4:** Data Assimilation Scheme (Particle Filter flow diagram).

Due to technical aspects relating to reinitialization of the process model that could not be resolved in good time, a modified form of the SIR-PF assimilation framework was implemented in this study where the background particles were drawn from pre-compiled look-up tables (LUTs) as illustrated in [Figure 19](#). Further details on the applied method are given in section [4.5.2](#).

### 3.9. Performance Metrics

Objective functions used for the assessment of the results obtained from various aspects of this study include the Root Mean Square Error/Difference (RMSE/D), Nash Sutcliffe Efficiency (NSE), standard deviation ( $sd$ ;  $\sigma$ ) and correlation coefficient ( $Corr$ ). These statistical measures are expressed as follows;

$$RMSE/D = \left[ \frac{1}{N} \sum_{i=1}^N (X_{sim}^i - X_{ref}^i)^2 \right]^{0.5} \quad (33)$$

$$NSE = 1 - \frac{\sum_{i=1}^N (X_{sim}^i - X_{ref}^i)^2}{\sum_{i=1}^N (X_{ref}^i - \overline{X_{ref}})^2} \quad (34)$$

$$sd(\sigma_{sim|ref}) = \left[ \frac{1}{N} \sum_{i=1}^N (X_{sim|ref}^i - \overline{X_{sim|ref}})^2 \right]^{0.5} \quad (35)$$

$$Corr = \frac{1/N \sum_{i=1}^N (X_{sim}^i - \overline{X_{sim}})(X_{ref}^i - \overline{X_{ref}})}{\sigma_{sim}\sigma_{ref}} \quad (36)$$

where  $X_{sim}$  and  $X_{ref}$  are the model and reference variables respectively;  $N$  is the data series' population;  $\overline{X_{sim}; ref}$  denote the mean values.

The centred RMSE/D as used in Taylor diagrams differs from the standard RMSD Equation (33) in that it considers the averages so as to meet the cosines condition ( $RMSD_{s,r}^2 = \sigma_s^2 + \sigma_r^2 - 2\sigma_s\sigma_r Cor_{s,r}$ ) inherent in the geometric design of the diagrams (Taylor, 2001);

$$centered\ RMSD = \left[ \frac{1}{N} \sum_{i=1}^N ((X_{sim}^i - \overline{X_{sim}}) - (X_{ref}^i - \overline{X_{ref}}))^2 \right]^{0.5} \quad (37)$$

where all terms are as previously defined.

## 4. RESULTS AND DISCUSSION

### 4.1. CRP Measurements Correction

The observed fast neutron counts were corrected for atmospheric pressure, atmospheric water vapor (absolute humidity) and incoming cosmic radiation to ensure the counts can reasonably infer SWC in the footprint. The correction was effected by applying Equation (10).

For derivation of the water vapor correction factors ( $f_{wv}$ ), a reference absolute humidity ( $\rho_{v0}^{ref}$ ) of  $0 \text{ gm}^{-3}$  was used while the average atmospheric pressure over the sampling period was taken as the reference ( $P_0 = 672.81 \text{ hPa}$ ) for the pressure correction factors ( $f_p$ ).

Peng (2017) performed sensitivity analysis for selecting a smoothing period that would yield optimal performance where they concluded that a 24-hour period gave the best assessment metrics (see [Appendix B](#)). Their study nonetheless settled on a 6-hour moving average period owing to the significance of the temporal resolution. In this study, however, the *Savitzky-Golay* filter (Savitzky & Golay, 1964) was implemented using a 24-hour smoothing window. The *Savitzky-Golay* filter addresses the temporal resolution aspect considered in Peng (2017) in that it applies a Least Squares fitting method that utilizes time as the independent variable.

For the smoothing filter, sets containing 96 data points, which represent 24 hours since the CRP provides measurements every 15 minutes, were fitted using the least squares criterion. This was implemented iteratively. For each iteration, the rightmost abscissa (x axis) value in the set (i.e. 96) was input in the resulting first order least squares equation giving the smoothed neutron count. This procedure was repeated for the other sets of datapoints by fitting linear regressions for each smoothing set until the entire data series was smoothed.

Variations of atmospheric pressure over the observation period, corrected fast neutron counts and smoothed cosmic neutron counts timeseries for the period prior and up-to the sampling campaign are illustrated in [Figure 5](#).

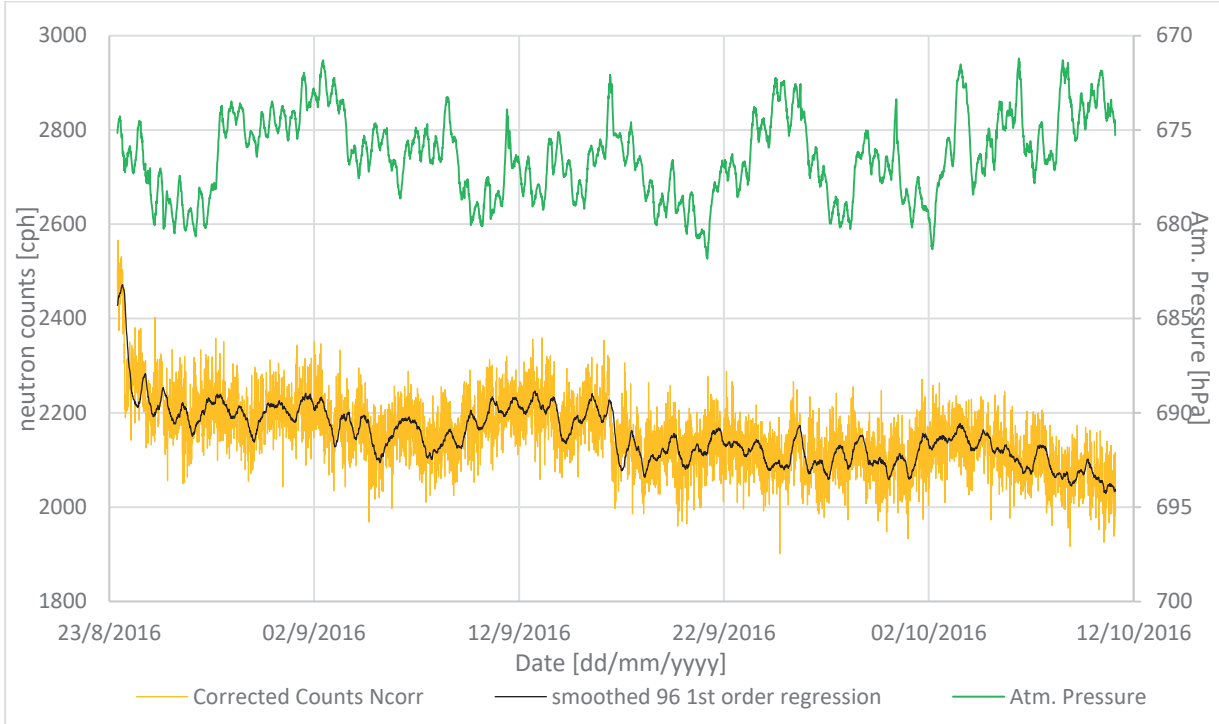


Figure 5: Corrected counts, air pressure timeseries.

#### 4.2. $N_{he}$ COSMIC Tuning

The COSMIC code as given in Equation (19) requires the calibration of the high energy (HE) neutron intensity parameter,  $N_{he}$ . To this end, observed SWC (from in-situ SM sensors) was used in the COSMIC code and the  $N_{he}$  parameter tuned until the simulated counts converged to the CRP observed counts. An optimized  $N_{he}$  of 654.963 was obtained. The SWC utilized in the calibration was from a period when the TSWC, as observed by the CRP, is equal to the USWC measured in-situ i.e.  $ST > 0$  °C.

Using the calibrated site-specific parameter  $N_0$  (retrieved in section 4.3) as input for Equation (25) yields a high energy neutrons parameter ( $N_{he}$ ) of 642.223. The optimized value (654.963) was therefore deemed to be within the feasible range and consequently used as the ‘true’  $N_{he}$  value in other parts of this study where the COSMIC model was utilized.

#### 4.3. Averaging and $N_0$ Retrieval

Previous research undertaken by Peng (2017) based the calibration of the site specific parameter,  $N_0$ , on equally weighted SWC averages which ignore the non-linear creation and attenuation of cosmic-ray neutrons related to depth and distance from the probe (i.e. layers/profiles close to the probe, both in depth and horizontally, contribute most of the neutrons detected at the CRP). The conventional weighting as proposed by Franz et al. (2012), conventional non-linear vertical by Bogena et al. (2013), and the revised method by Schrön et al. (2017) were tested on the sampling campaign dataset yielding footprint averages of 0.4777

$m^3m^{-3}$ ,  $0.4049 m^3m^{-3}$  and  $0.4267 m^3m^{-3}$ , respectively while the uniform averaging (equal weighting) method gave  $0.3361 m^3m^{-3}$ .

For verification, COSMIC was used as the “reference”<sup>1</sup>. The averaged SWCs derived using the different weighting/averaging methods were compared against the COSMIC derived SWC averages, i.e. utilizing layer weights as computed by COSMIC. The Nash Sutcliffe Efficiency (NSE) coefficient, a measure used to quantify goodness of fit, mean error (ME) and the root mean square error (RMSE) were used.

Whereas the conventional and revised weighting methods attained NSE coefficients of 0.98 and 0.97 and RMSEs of  $0.003 m^3m^{-3}$  and  $0.004 m^3m^{-3}$ , respectively, the equally weighted method achieved an RMSE of  $0.038 m^3m^{-3}$  and an NSE of -1.67 which is way below the threshold (0.6) deemed satisfactory. Statistical metrics for the different averaging methods as compared to COSMIC are shown in [Figure 6](#). It should be noted that in Taylor diagrams, the (centred) Root Mean Square differences are derived using Equation (37).

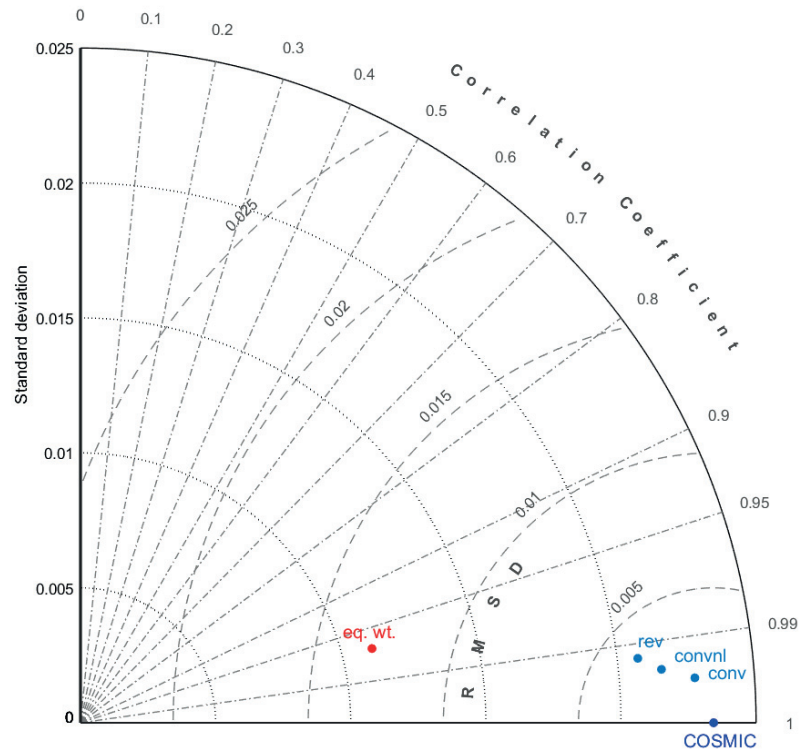


**Figure 6:** Taylor diagram showing comparison of COSMIC derived SWCs with those from equal, conventional and revised weighting approaches over the August to October, 2016 period.

[Figure 7](#) shows cumulative weights over depths using the different averaging methods where it is evident that the conventional non-linear averaging method assigns weights similar to COSMIC with  $\approx 86\%$  being assigned to uppermost layers (*above*  $Z^*$ ). The weights for all soil layers were calculated using Equations (1) and (4) for the uniform and conventional non-linear vertical methods, respectively. Since dataset from only one soil moisture probe was used, the horizontal weight, as given by Equation (2), was inconsequential in the iterative weighting process. The weights as assigned by COSMIC were similarly derived after running

<sup>1</sup> In this study, the COSMIC computed counts showed good similarity with the measured CRP counts ( $r = 0.84$ ) though some limitation could be observed as the counts were simulated using SWC measurements from one in-situ sensor thus neglecting the spatial variation of SWC over the footprint.

the model (COSMIC returns weights as part of the output). The weights were then cumulatively summed and [Figure 7](#) plotted.

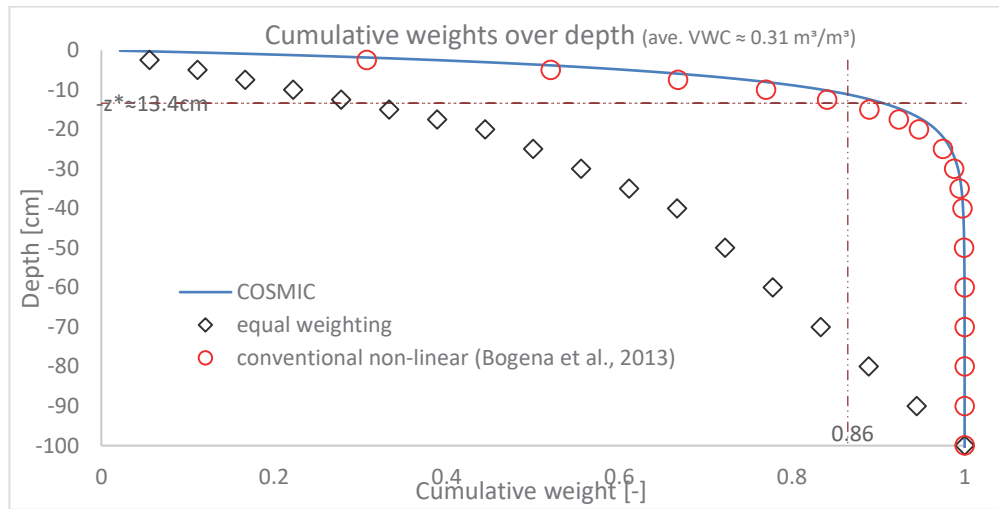


**Figure 7:** Cumulative weights over depth (uniform vs conventional vs COSMIC) [Observed SWC-11·10·2016 23:45]

It is worth noting that, Equation (9) with the input of the average SWC as derived using the conventional non-linear method ( $0.31 \text{ m}^3/\text{m}^3$ ) yields a  $Z^*$  of 13.38cm as illustrated in [Figure 7](#). Applying the equally weighted SWC ( $0.26 \text{ m}^3/\text{m}^3$ ) in the same equation yields 15.21cm, contradicting the value read from the plot ( $\approx 75\text{cm}$ ). The equal weighting method is therefore not recommended in this study.

The cumulative weights over depth, as calculated using the conventional non-linear method, for different average SWCs are shown in [Figure 8](#);

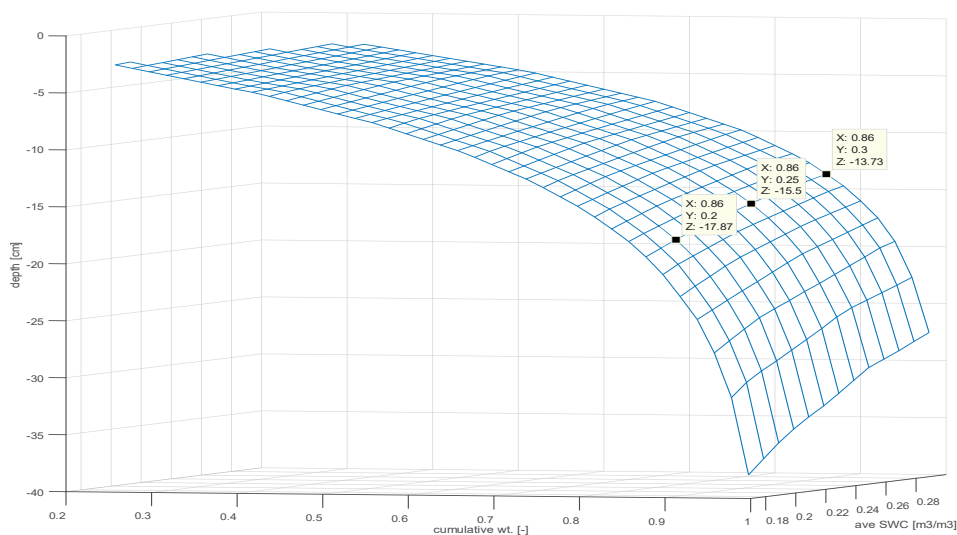


**Figure 8:** Surface plot showing the CFoC over depth for different SWC averages.

To select between the revised and conventional averaging methods, the SWC inferred from CRP counts (calculated using Desilets et al.'s (2010) equation) was taken as the reference for inter-comparisons, i.e. SWCs derived from using the revised  $N_o$  (calibrated using revised sampling average) and conventional  $N_o$

(calibrated using conventional sampling average; both linear and non-linear vertical) were compared against the reference.

The conventional (non-linear vertical) weighting yielded the lowest RMSE ( $0.063m^3m^{-3}$ ) thus selected for the retrieval of the site-specific calibration parameter  $N_0$  (i.e. 3939.38 cph). This relatively high RMSE (compared to RMSE calculated with COSMIC-SWC as reference) is likely due to the use, in the weighting, of one in-situ measurement to represent the heterogenous CRP footprint. Selection of the conventional non-linear method is in line with Baatz et al. (2015) who concluded that the averaging approach considers and assigns weights similar to the COSMIC operator. [Figure 9](#) shows the timeseries of CRP-observed and COSMIC-calculated neutron counts, together with the derived SWCs using Desilets et al.'s (2010) equation, uniform, revised and the conventional (both linear and non-linear vertical) methods, respectively. Bias was computed by subtracting the “reference” from modelled (equal, conventional and revised weighting) values.



**Figure 9:** a) Neutron counts, SWC timeseries; b) bias, mean bias (ME) for the different weighting methods.

From [Figure 9b](#), it can be noted that with gradual change in average SWC, both the conventional and revised weighting approaches properly mimic COSMIC weights while abrupt changes in the prevailing SWC conditions lead to observable deviations/differences in weighting. On the other hand, the equally weighted series is always underestimating the averages since it assigns similar weights to all layers i.e. lower layers are assigned equal weights as top layers.

#### 4.4. Reference Soil Ice Content

Soil Ice Content (SIC), against which the modelled SIC states were to be validated, was computed using Equation (18) where soil water inferred from the CRP neutron counts (using Equation (14)) was taken as the TSWC and the averaged in-situ sensor measurements as the USWC. The USWC over the sensing depths were weighted using the selected conventional non-linear vertical method. The ‘true’ SIC for the January-to-March 2016 winter period is illustrated in [Figure 10](#) below;

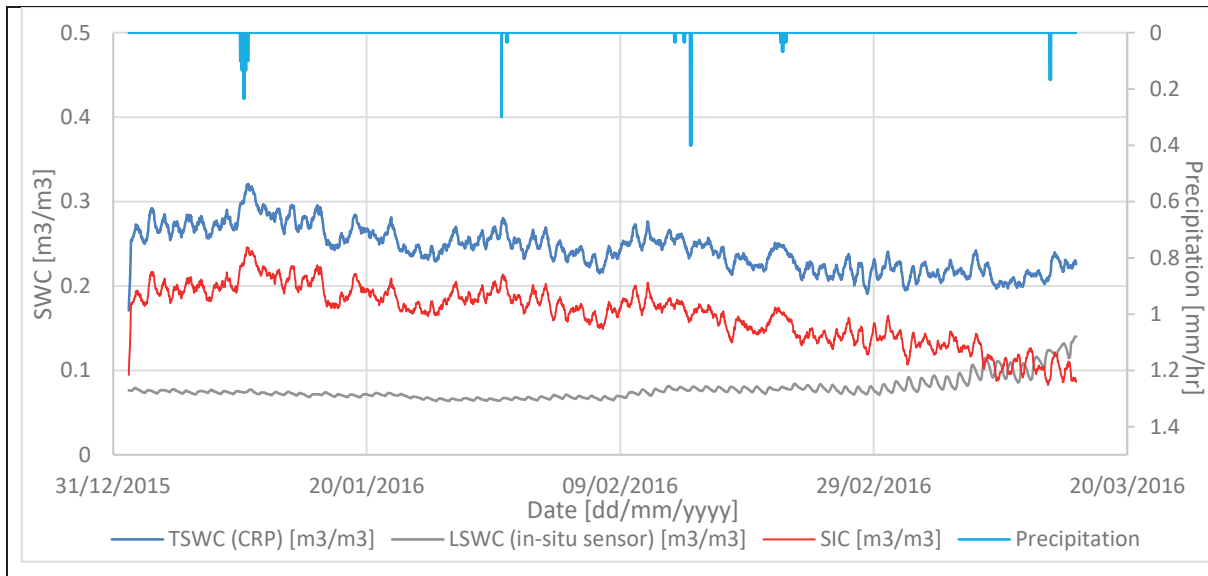


**Figure 10:** SIC ‘truth’ timeseries as well as the average TSWC inferred from CRP corrected counts and average USWC derived by averaging in-situ SM probe observations using the conventional non-linear weighting method.

#### 4.5. Data Assimilation: Particle Filtering

Given the highly non-linear nature of equations solved in the numerical STEMMUS-FT model as well as non-linearity of the COSMIC model, a data assimilation scheme based on the particle filter, which can handle non-gaussian error propagation and non-linearity exhibited in environmental processes, was preferred and consequently implemented. All assimilation experiments herein assume equal spatial scale between observations (states and forcing data) and model simulations i.e. univariate single-scale – UVSS DA (Montzka et al., 2012).

##### 4.5.1. Heuristic COSMIC Experiment

Initial assimilation experiments were set up where CRP observed measurements were assimilated after every 15 minutes for bias correction of COSMIC simulated counts over the period utilized in the SWC averaging and  $N_0$  retrieval ( August to October, 2016; see [Figure 9](#)). The observed soil moisture measurements, which serve as input (‘forcing’) for the COSMIC observation model, were initially disturbed to have 1000 particles around the observations (taken as the ensemble mean) and assuming a normal distribution with an uncertainty range of  $\pm 0.02 m^3 m^{-3}$  as given in Dente et al. (2012).

The CRP observations were also perturbed to have a similar number of particles with mean and variance equal to the observed counts (neutrons follow Poisson distribution (Zreda et al., 2012)). Two experiments were set up, i.e. updating of states only and state-Nhe parameter updating.

The pre-compiled data pool of ensembles, as detailed in the preceding paragraph, was utilised in carrying out the DA implementation. This was performed by following the SIR-PF framework as illustrated in [Figure 31](#)/[Figure 19](#). The SWC particles used as input for COSMIC were generated by globally perturbing the measurements following the procedure detailed in sub-section [4.5.2.2](#). The joint state-Nhe assimilation, in addition to assimilating the CRP observations, incorporated the tuning of the high energy parameter as is shown in the flow diagram given in [Appendix C](#) ([Figure 31](#)).

For state-only updating, the Nhe parameter was set to the manually calibrated value (654.963) and the PF then implemented by assimilating the ensemble of observed neutron counts. The resulting time series is shown in [Figure 11](#). In the joint state-parameter DA scenario, an ensemble of false Nhe parameters (mean and variance = 300) was initialized to test the PF's capability in estimating/tuning parameters.

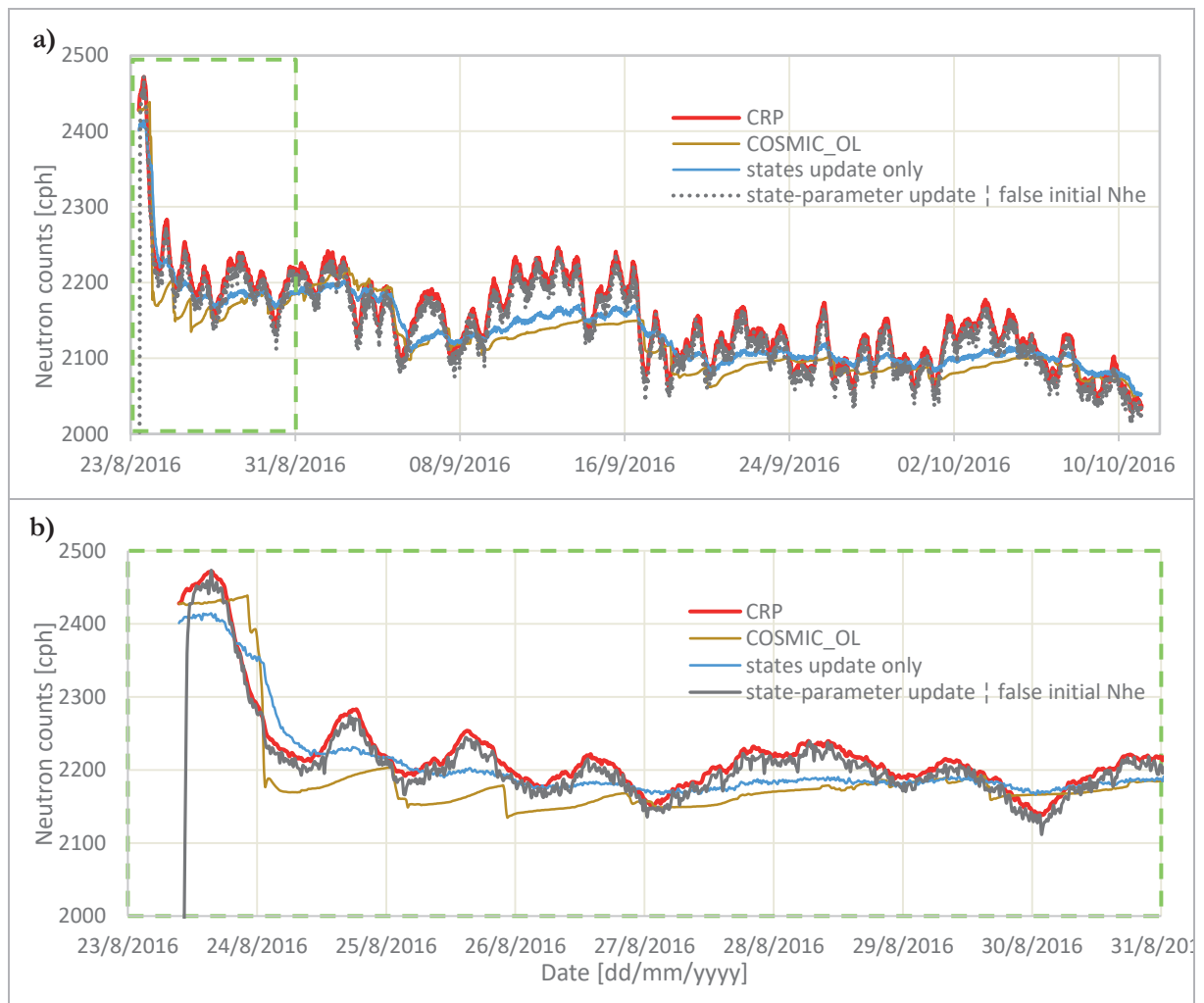


**Figure 11:** a) State & state-parameter updates versus open loop (without DA) over the Aug-Oct 2016 period; b) zooming in to the first week of the data series.

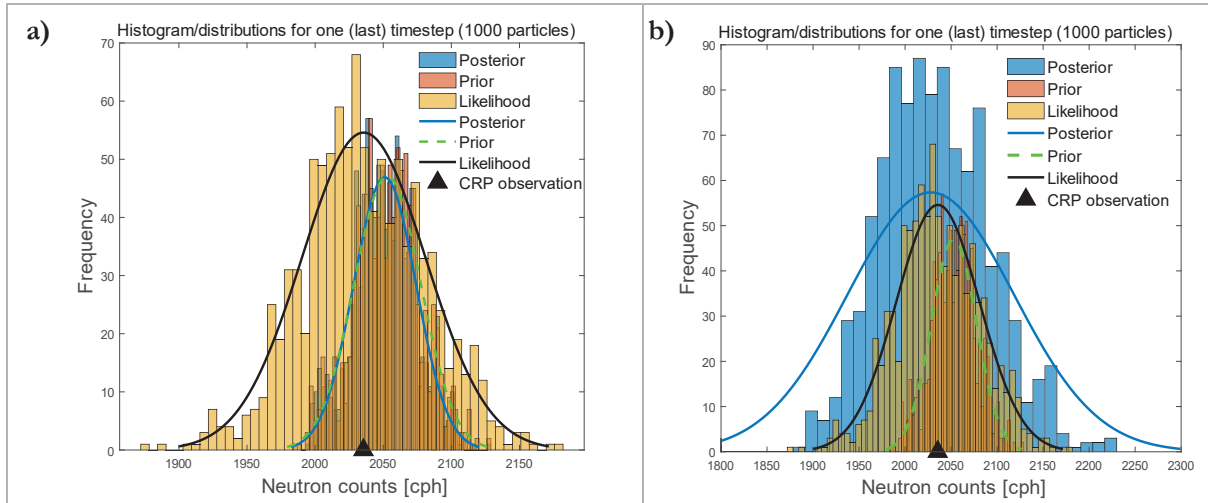


**Figure 12:** Histograms for the last timestep: **a)** states update only and **b)** states-Nhe parameter update.

In the state-only update for the last timestep (Figure 12a), a best estimate of 2051.174 cph was derived compared to an open loop simulated value of 2053.09 cph (CRP observation=2035.491 cph). No meaningful correction could be achieved as the whole prior ensemble was contained in the likelihood set. Another state-only test was performed utilising unperturbed CRP observations to establish if this could lead to improved corrections. A slight improvement of the correlation between the analysis and measurements was observed i.e. from 0.89 to 0.92. The best estimate for the last timestep was however found to be similar to what was obtained with perturbed observation (2051.32 cph). There was therefore no marked difference between the outcomes derived from use of perturbed and unperturbed CRP observations.

The above finding concurs with Evensen (2003) who pointed out that whether one updates using perturbed or the first-guess observation is an arbitrary decision. That notwithstanding, Evensen (2003) recommended the use of perturbed observations since that allows creation of ensembles with correct error statistics. Both strategies have been applied in previous studies. Han et al. (2016), for instance, utilized perturbed likelihood (neutron counts) in their study while Montzka et al. (2011) implemented a particle filter utilizing unperturbed observations (SM states). As will be shown later (section 4.5.2.3), assimilation of unperturbed measurements seems to outperform DA with perturbed observations.

The COSMIC model requires tuning of the high energy parameter which is then used in derivation of simulated fast neutrons reaching the probe given the prevailing SWC (hydrogen pool) conditions. It is common practice to assume this calibrated value as time invariant. On the other hand, since the incoming cosmic rays are more than likely to fluctuate over time, this high energy neutrons parameter at the surface is also likely to exhibit temporal variation, hence the motivation to carry out an illustrative joint state-parameter DA experiment.

Figure 12b shows the last timestep's histogram where the joint state-Nhe setup attained an analysis estimate of 2027.9 cph. Evolution of the Nhe analysis over the period is illustrated in Figure 13 with an average, for

the entire period, of 656.965 which is quite close to the manually calibrated  $N_{he}$  hence showing that it is possible, through a joint state-parameter DA, to tune an initial false parameter to within the ‘true’ range. However, the capability of the filter in correcting for inaccurate parameterization is dependent on the ‘false’ value being within a reasonable range.

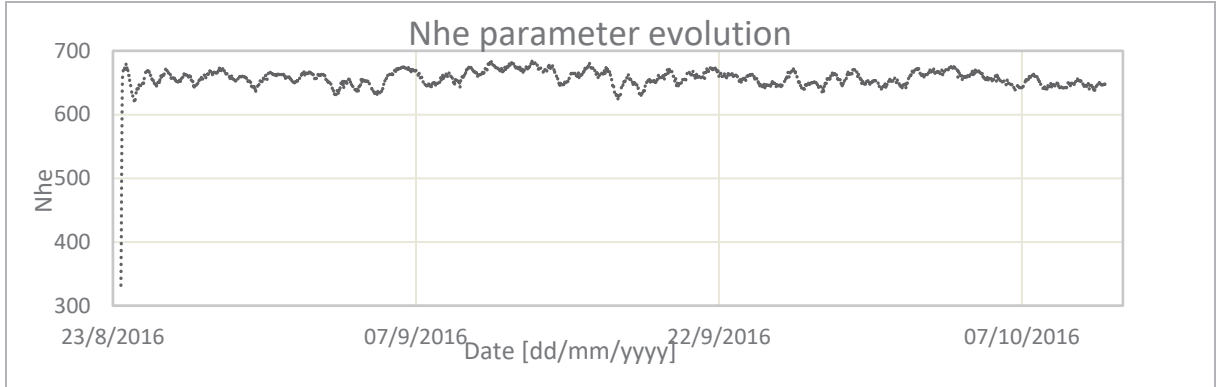


**Figure 13:** Evolution of the site-specific high-energy calibration parameter ( $N_{he}$ ).

The seemingly abrupt correction over a short period is due to the broad spread of parameter particles in the relatively large ensemble. Since  $N_{he}$  is assumed to follow Poisson statistics, some of the particles will likely be close to the optimal value and will be allotted high weights during initial corrections. For example, the false  $N_{he}$  mean of 300 has a standard deviation of 17.32 (square root of the mean), which increases after every ensemble run, leading to the attainment of the optimal  $N_{he}$  within a short time span.

[Figure 14a.](#) and [Figure 14b.](#) show initialization with totally inaccurate  $N_{he}$  values i.e. 50 and 1500 where it is evident that the filter performs poorly (a.) while in (b.) the parameter correction fails *in toto* i.e. the simulated counts are entirely out of sync with the CRP measurements.

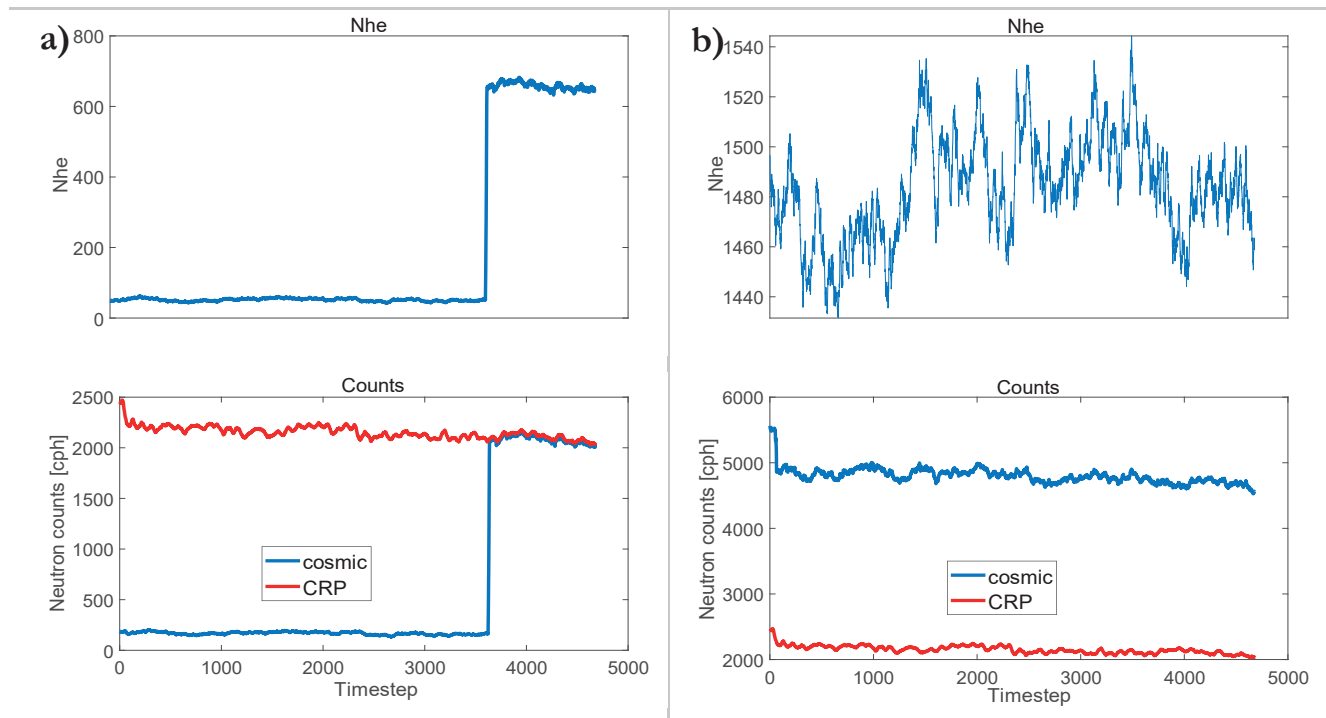


**Figure 14:** False  $N_{he}$  initialization a) 50 and b) 1500 and the corresponding neutron counts timeseries.

It should however be noted that these illustrative experiments employ a relatively parsimonious model (COSMIC) where only one parameter (the high energy parameter- $N_{he}$ ) is tuned while other parameters, i.e.  $L_1$ ,  $L_2$ ,  $L_3$  (a function of soil bulk density),  $L_4$  and  $\alpha$  (also a function of bulk density), are taken to be constant. As such, any  $N_{he}$  value that is within range will tend to always correct any observable differences between simulated (COSMIC) and observed (CRP) counts since the most optimal  $N_{he}$  is assigned the highest weight in the particle filtering process leading to close tracking of the likelihood.

#### 4.5.2. Model (STEMMUS) Scenarios

Due to issues experienced during the coupling of STEMMUS and COSMIC models in the data assimilation scheme, a method similar to one termed Observing System Experiment (OSE) by Moradkhani (2008) was established. OSEs are described as DA implementations established with an aim of allowing the examination of assimilation processes and generally involve the use of simulated data-sets of terrestrial model states (Moradkhani, 2008). These data-sets can be derived by running the process model with different parameterizations, initial, boundary and/or forcing conditions. Although with a slightly different goal, a similar concept is applied in the generation of ensemble forecasts by the European Centre for Medium-Range Weather Forecasts (ECMWF) where 51 separate forecasts (50 perturbed members and one unperturbed control forecast (CTRL)) are derived using different starting conditions (Owens & Hewson, 2018).

From above descriptions, the pre-compiled data pools need to consider the various sources of modelling uncertainties. In this study however, other than the initial soil moisture states, attempts to change other model aspects led to complications that, unfortunately, could not be reasonably resolved in a timely manner. As such, in addition to utilizing the data-set compiled from model integrations, data pools compiled from random global perturbations (model uncertainty) were used in the assimilation scenarios and thus presented.

Equation (26) envisages the existence of a model error which should be able to account for the various uncertainties present in the modelling process. In most assimilation studies, the model error is disregarded as it is assumed that it is addressed by having considered uncertainties occasioned by forcing data, model parameters, etc. For example, in Zhang et al. (2017) where a joint state-parameter assimilation was undertaken using the VIC and CLM models, a value of zero for the model error was used since it was assumed that “uncertainty was captured by uncertain model parameters and model forcings”. In this study, however, arbitrary model uncertainties, in the form of random global perturbations, were also assumed to represent the existing parameters, structure and forcing data uncertainties. It was thus assumed that the prevailing modelling uncertainties will fall within these uncertainty ranges.

This approach, although not common, allowed integration of observed cosmic-ray fast neutron observations and subsequent investigation of the assimilation framework. The aforementioned model

complications need to be addressed to enable the carrying out of more “standard” data assimilation investigations.

Results for these scenarios are presented in the next sub-sections. First, the open loop (calibrated model run without updating) results are presented. The open loop simulations are then used to compile ensemble pools with arbitrarily assumed model uncertainty ranges of  $0.1m^3m^{-3}$  and  $0.05m^3m^{-3}$  for further discussion. Finally, results from a DA set-up utilizing a data pool compiled from model integrations with different initial soil moisture states are analysed.

#### 4.5.2.1. STEMMUS-FT Open Loop (SFT-OL)

This section reports on reproduced work from Yu et al. (2018). Here the Clapeyron and van Genuchten model was applied for the derivation of the SWC with initial states and boundary conditions as at 1<sup>st</sup> December 2015, and forcing data from December 2015 to 15<sup>th</sup> March 2016 used for initializing the model. The simulated USWC, averaged using the conventional non-linear method, is shown in [Figure 15](#). It should be noted that only results from January 2016 are presented herein as CRP observations were unavailable prior to this date.

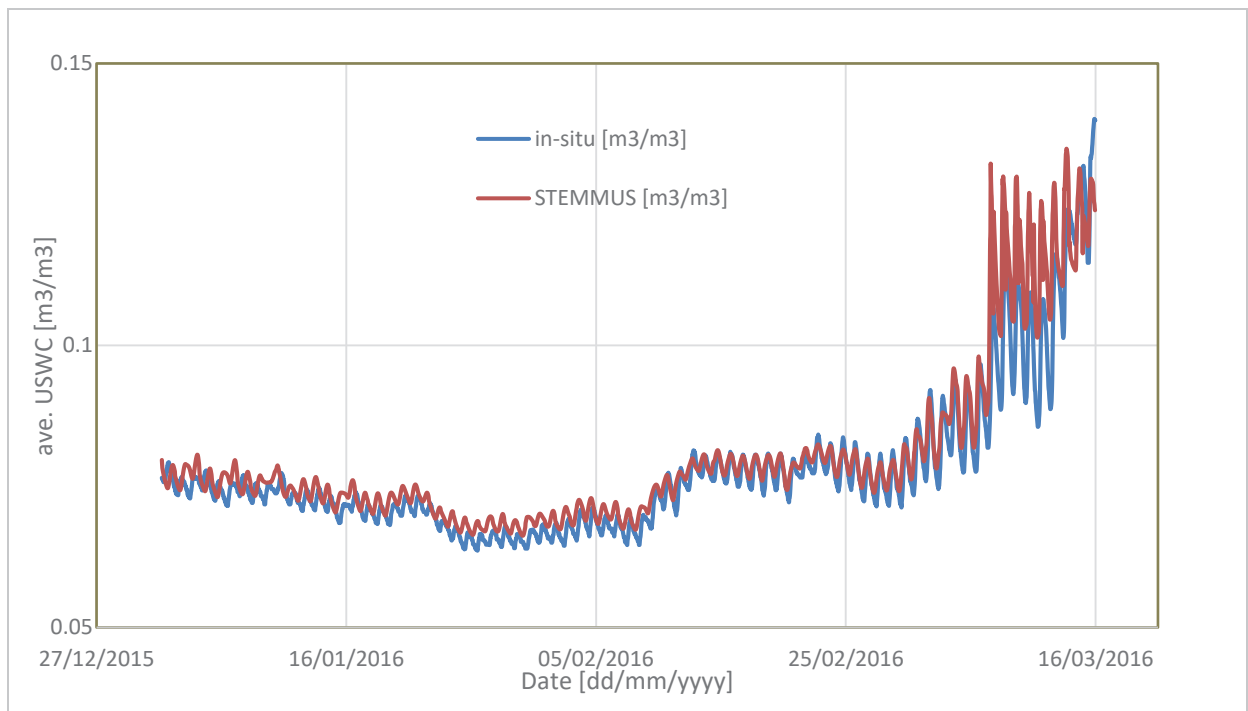


**Figure 15:** Average USWC applying the conventional non-linear method (average for the CRP footprint).

The simulated average USWC over the CRP’s effective sensing depth yielded a positive correlation of 0.96 to the observed average with an RMSE of  $0.0051m^3m^{-3}$  and an NSE of 0.851. [Figure 16](#) shows a scatterplot for the average simulated USWC against the observed averages where the model shows capability of simulating USWC states below  $0.1m^3m^{-3}$  with relatively good accuracy while largely overestimating USWCs above  $0.1m^3m^{-3}$ . Since the effective depth as determined by the conventional non-linear method

consists mainly of top soil layers, a possible explanation for this observation is the overestimation of USWC by the model at the 10 cm layer for ST greater than  $-2^{\circ}\text{C}$  as illustrated by the SFCC ([Appendix D; Figure 32](#)).

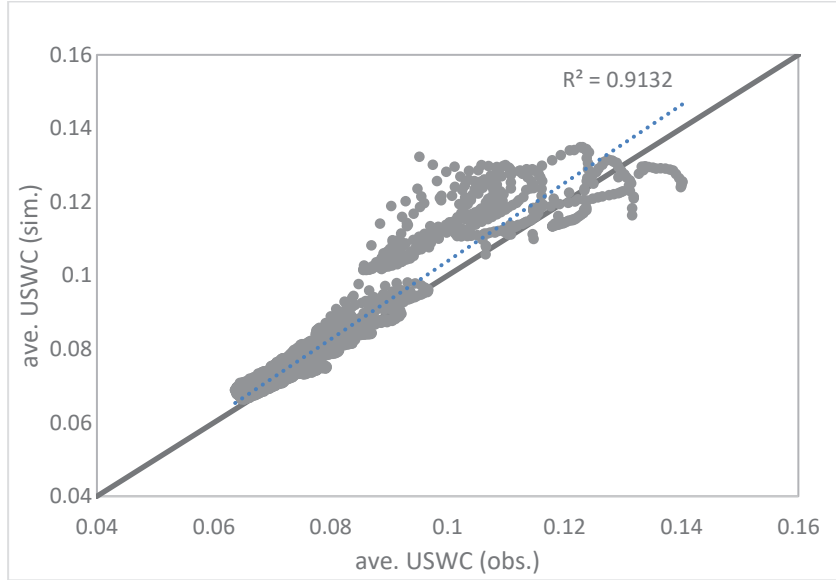


**Figure 16:** Scatter diagram showing the simulated against observed USWC (averaged using the conventional non-linear method).

[Table 4](#) below lists metrics computed for different observation layers. Timeseries' of simulated and observed ST states as well as their corresponding SFCCs over the 5, 10, 20, 40 and 80 cm layers are presented in [Appendix D](#).

**Table 4:** Simulated-vs-observed states RMSE and Correlation coefficients.

Depth [cm]	RMSE		NSE		Correlation coeff. (r)	
	USWC [m <sup>3</sup> /m <sup>3</sup> ]	ST [ $^{\circ}\text{C}$ ]	USWC	ST	USWC	ST
5	0.011	1.34	0.803	0.582	0.897	0.793
10	0.008	0.82	0.659	0.758	0.957	0.891
20	0.004	0.29	0.768	0.934	0.983	0.969
40	0.006	0.61	-0.037	0.243	0.936	0.989
80	0.002	0.12	0.938	0.926	0.978	0.983

The root mean square difference of the USWC and ST states indicates the better model performance with depth. This pattern, however, is disrupted at the 40 cm soil layer, which could be due to the sharp soil texture change at this depth as observed by Yu et al. (2018). The soil texture change is also the likely cause of inconsistencies observed in the 40cm-layer's SFCC, where different liquid water contents are observed by the in-situ sensors. Since soil texture is one of the parameters that influence the determination of soil

water (Matula et al., 2016; Rowlandson et al., 2013), a possible solution to the observed inconsistencies would be to have the in-situ SM probe recalibrated to account for the characteristic change.

This effect is also illustrated by the difference/lag exhibited between the observed and simulated freezing-fronts at the 40cm depth. The fronts were derived by interpolating for soil depths with 0 °C (freezing point of water).

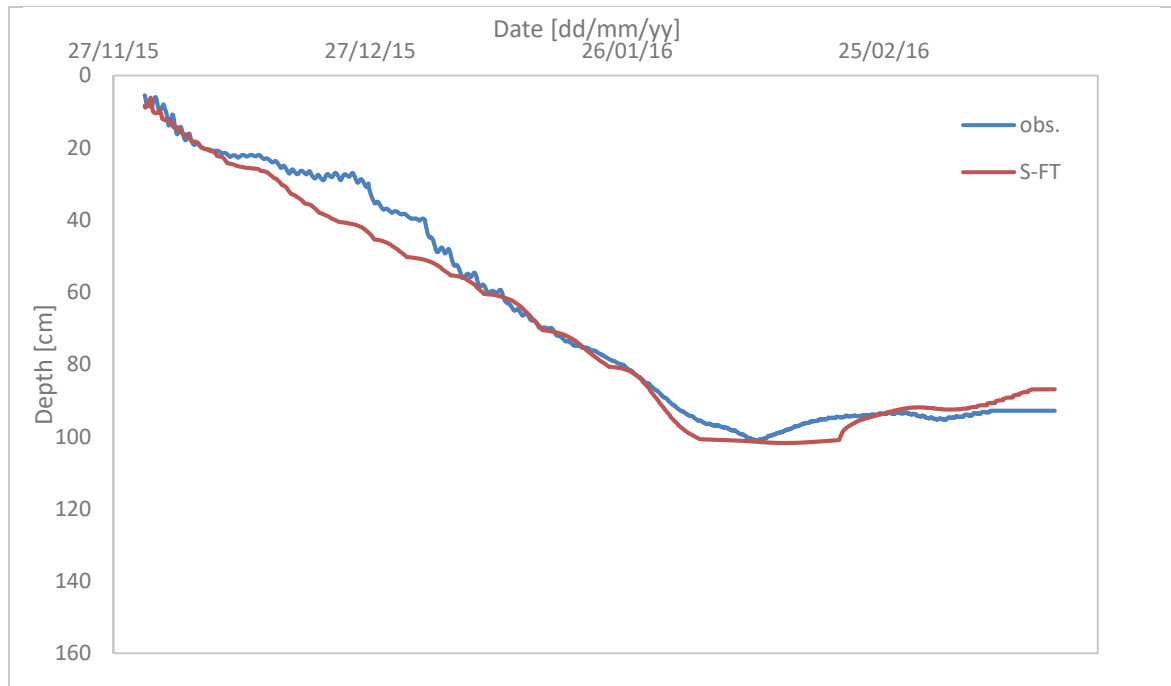


**Figure 17:** Observed and simulated freezing-fronts: reproduced from Yu et al. (2018).

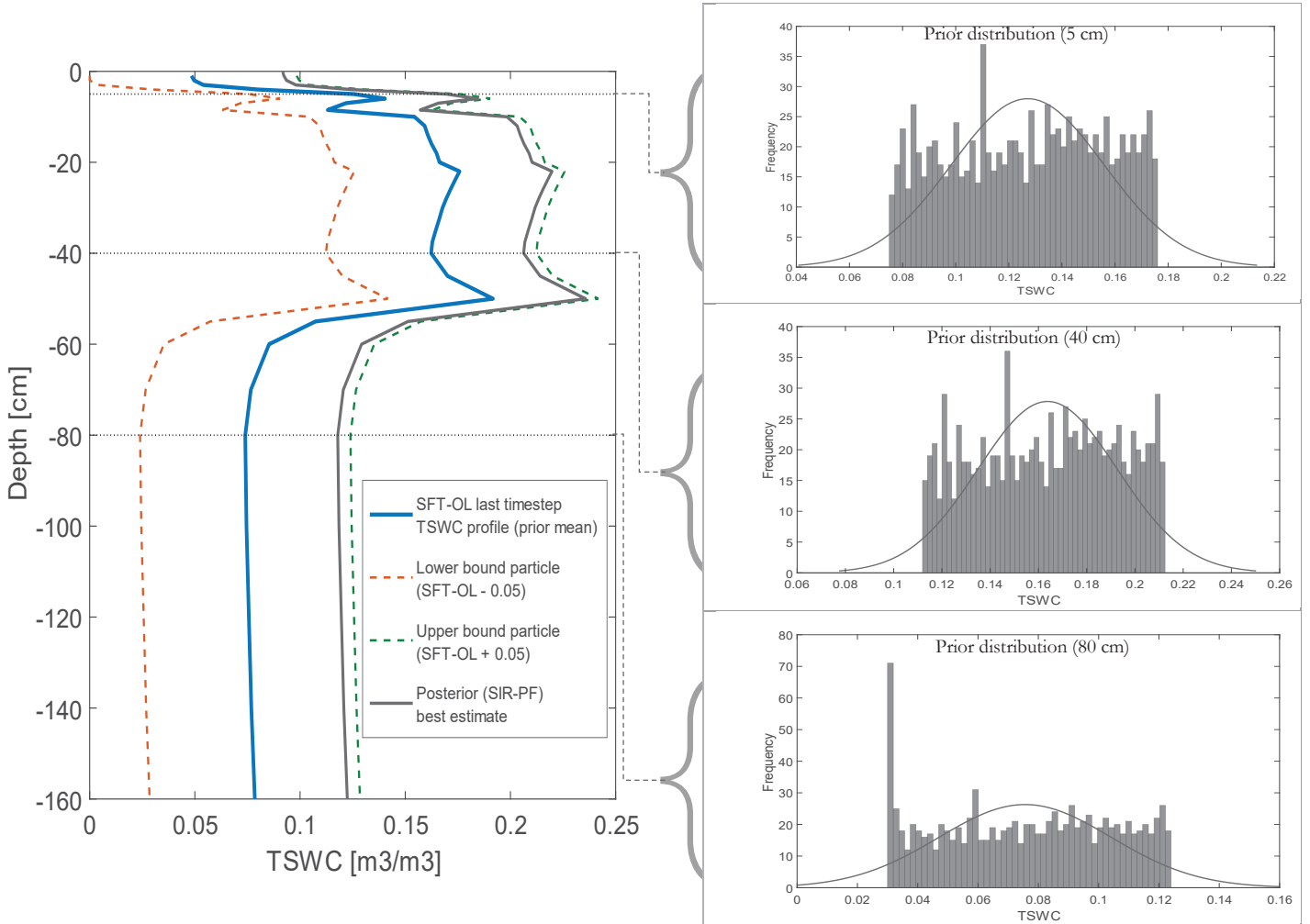
The model shows quite good capability of accurately simulating soil temperatures (ST) and the USWC. The assimilation experiments, presented later, were therefore only set up to update the TSWC and in consequence, the SIC. Another reason for only updating the TSWC was the univariate nature of the DA scheme where only the CRP measurements (proxy of TSWC) were assimilated. It was therefore assumed that ST and USWC states track the observation closely, hence the need for only updating the total soil water.

#### 4.5.2.2. Globally Perturbed TSWC Setup

The simulation dataset obtained from the Open Loop (SFT-OL) was used for DA experiments in this subsection. The TSWC simulations were globally perturbed to have 1000 ensemble members with uncertainty ranges of  $\pm 0.05 m^3 m^{-3}$  and  $\pm 0.1 m^3 m^{-3}$ . Global perturbation, where all modelled layers were disturbed with the same random factor selected from within the model uncertainty ranges, was done to ensure that particles in the Look-Up Table (LUT) of ensembles were consistent with model physics (i.e. conservation of the general soil water content trend in the soil column).

An illustration of how the global perturbation was performed for the last timestep while utilizing the  $0.05 m^3 m^{-3}$  uncertainty range is given in Figure 18. The red dotted SWC profile represents the lower bound

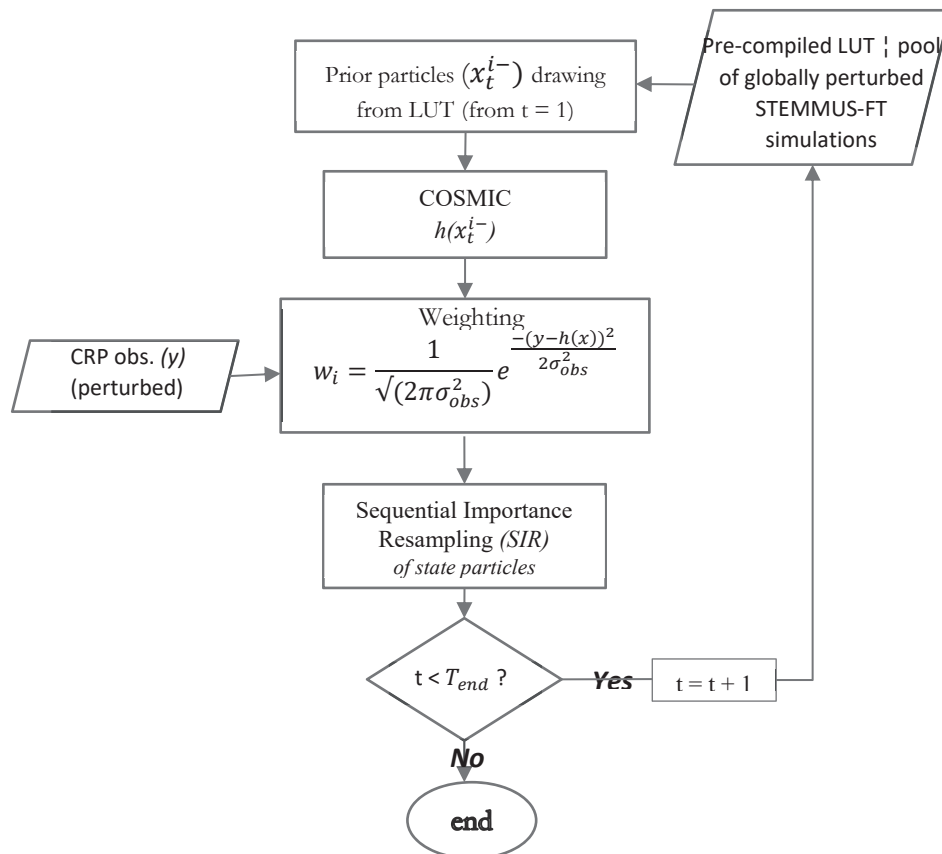
particle given by  $SFT-OL - 0.05m^3m^{-3}$  while the green dotted profile to the right is the upper bound particle given by  $SFT-OL + 0.05m^3m^{-3}$ . All other background particles were uniformly distributed within the two limits with a prior mean equal to the particle represented by the blue solid line.



**Figure 18:** Example illustrating the application of the  $0.05m^3m^{-3}$  uncertainty range global perturbation together with histograms for prior ensembles generated for the 5 cm, 40 cm and 80 cm layers (last simulation timestep).

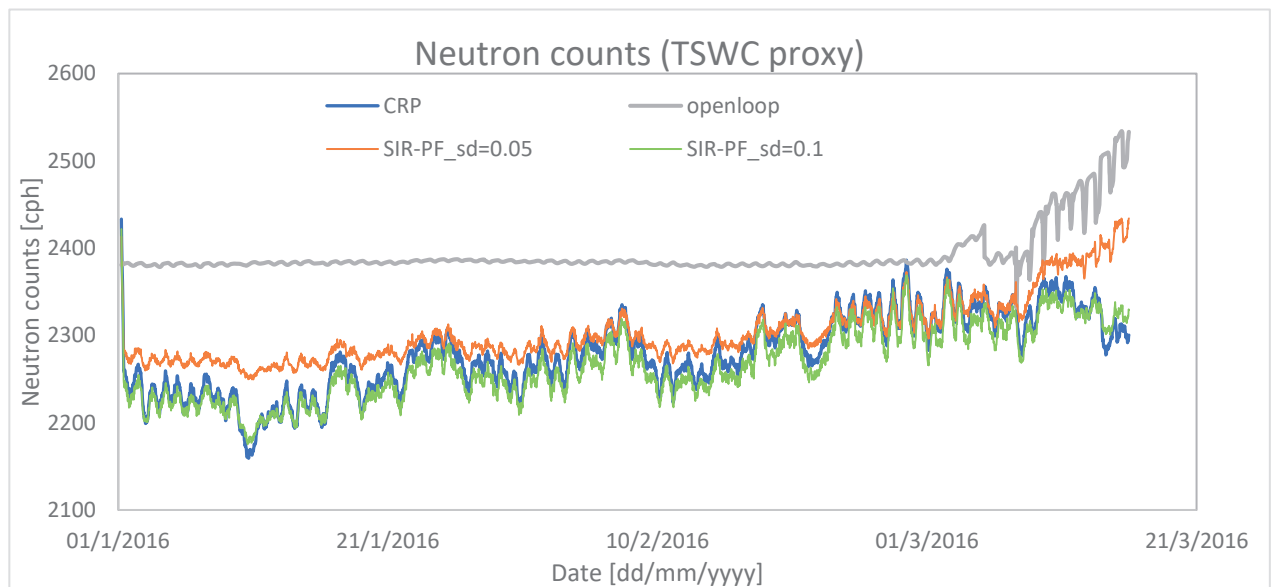
Although the three histograms exhibit a similar pattern (shape), the leftmost bin in the 80 cm histogram appears with higher frequency than in the other histograms. This is because a residual water content of  $0.03m^3m^{-3}$  was assumed and consequently set to reasonably limit the spread. The black solid line in the SWC profile diagram (Figure 18) shows the analysis best estimate for the last updated timestep (i.e. the mean of the SIR-PF derived posterior ensemble), where it is clear that the global perturbation datasets keep the physical consistency.

TSWC states from the standard 5, 10, 20, 40, 80 and 160 cm layers were then propagated through COSMIC for calculating neutron counts. These simulations were then used for particle weights computation and subsequent resampling in the SIR-PF implementation as illustrated by Figure 19.



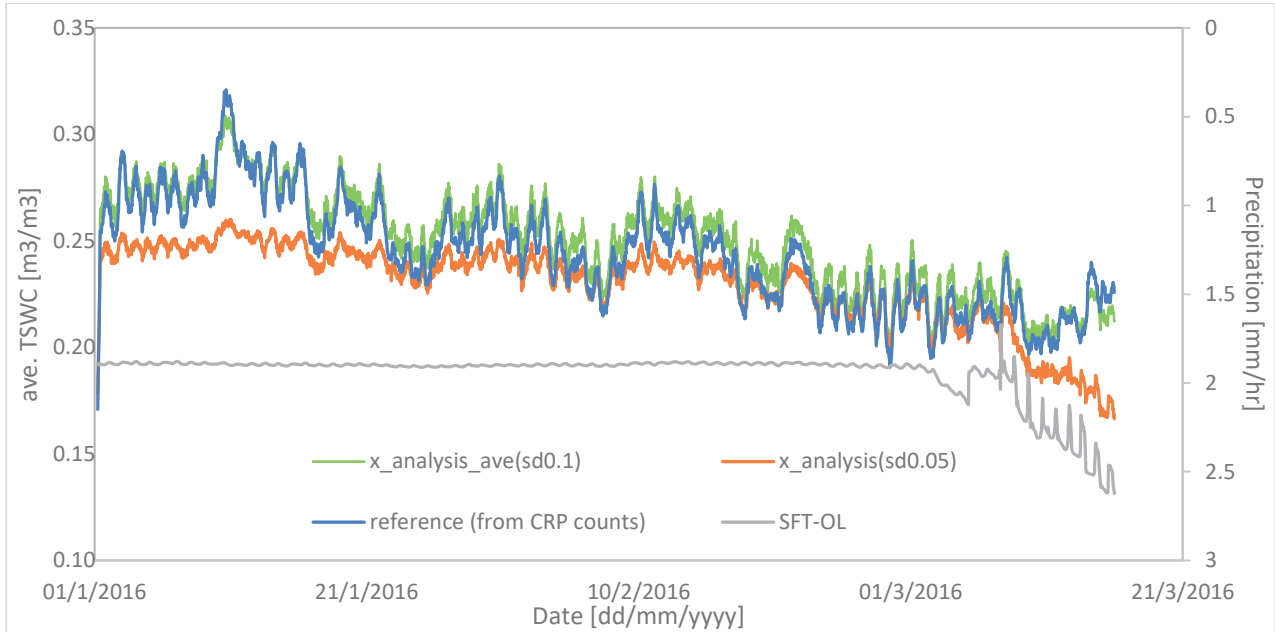
**Figure 19:** Data Assimilation Scheme (Particle Filter flow diagram) utilizing a pre-compiled look-up table.

Figure 20 below shows the timeseries of the prior counts (as computed from modelled (SFT-OL) states), likelihood (CRP observations) and the analyses.



**Figure 20:** Neutron counts timeseries: simulated open loop (OL), after the implementation of SIR\_PF (with  $\pm 0.1 m^3 m^{-3}$  and  $\pm 0.05 m^3 m^{-3}$  uncertainty ranges) and observed.

For consistency, the average TSWC used for comparison with the reference was derived by substituting the updated simulated counts into Equation (14). Similar to derivations in sub-section 4.5.2.1, the average USWC was derived by using the conventional non-linear vertical method. The timeseries showing the obtained water content states (total) are as below;



**Figure 21:** Average 'TSWC timeseries' (reference, OL and analyses).

The simulated counts timeseries (based on the open-loop TSWC) is relatively constant over a large part of the forecasted winter period. The small variations can be attributed to the effective density modifications made to the COSMIC code to account for the presence of frozen and unfrozen soil water. The SFT-OL counts do not, however, follow the CRP measurements as can be observed in [Figure 20](#) due to the model's underestimation of average TSWC over the effective sensing depth of the CRP (see [Figure 21](#)).

Rainfall, which acts as a source of hydrogen, has an effect on the neutron counts as all precipitating events lead to an observable reduction (moderation) of counts reaching the CRP. These precipitation effects on the soil water balance are however not reflected in the open loop model simulations as would be expected. The more pronounced variations in the observed neutron counts timeseries however suggest likely existence of other hydrogen sources that need to be further investigated.

Assimilating the observed neutron counts allowed the correction of the simulated states as shown in the resulting scatterplots given in [Figure 22](#). An overview of assessment metrics between updated counts (including those from SFT-OL) and the reference is presented in [Table 5](#).

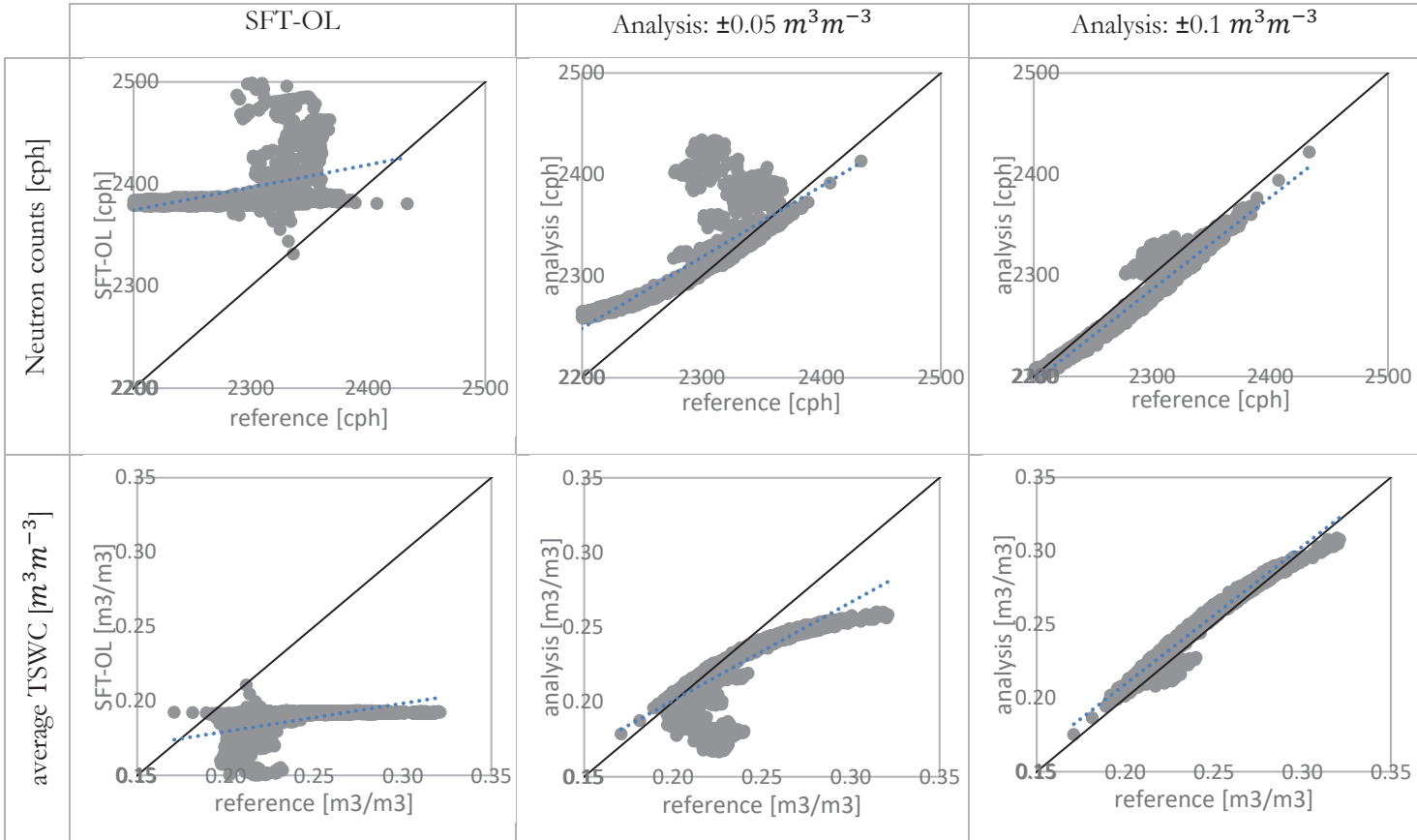


**Figure 22:** Scatter plots of simulated neutron counts and average TSWC against their respective reference (observed) states.

**Table 5:** Metrics for open loop and analysis scenarios.

	Neutron counts			Average TSWC		
	$r$	RMSE [cph]	NSE	$r$	RMSE [ $m^3m^{-3}$ ]	NSE
SFT-OL	0.358	120.758	-6.508	0.409	0.061	-4.808
$\pm 0.05m^3m^{-3}$	0.830	35.029	0.368	0.852	0.019	0.404
$\pm 0.1m^3m^{-3}$	0.983	15.027	0.884	0.984	0.008	0.898

Figure 23 illustrates the last timestep's histograms for the two global perturbation scenarios. The  $\pm 0.1m^3m^{-3}$  model uncertainty range gave an estimate very close to the CRP observation (i.e. analysis ensemble mean = 2329.16 cph; CRP observation = 2300.38 cph) since it provided enough spread that allowed resampling of most of the posterior from prior particles that were also members of the likelihood ensemble set (i.e. resampling was mostly from particles in the range of around 2250 cph to 2450 cph). The  $\pm 0.05m^3m^{-3}$  prior distribution returned an updated best estimate of 2434.11 cph.

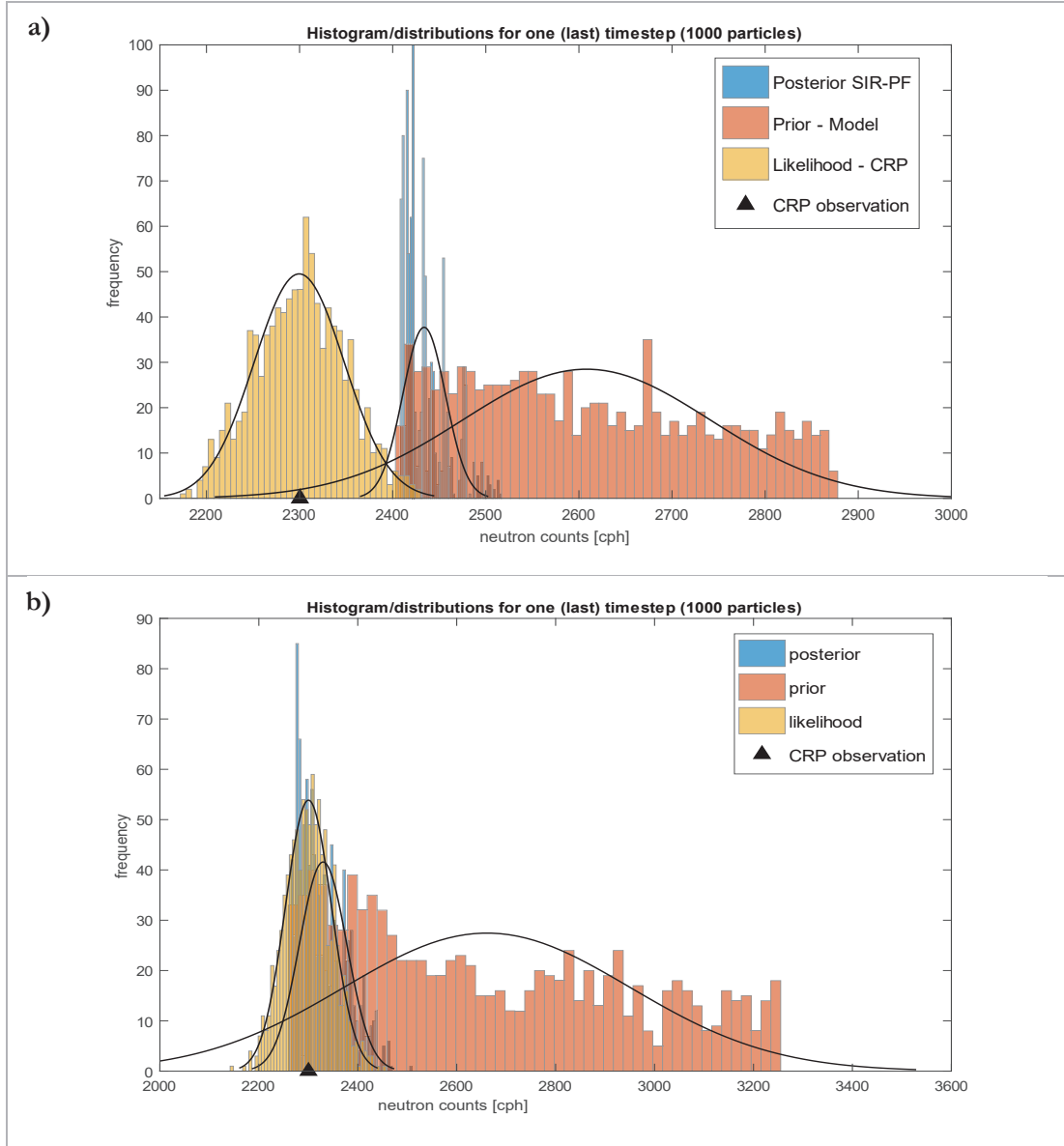


**Figure 23:** Posterior, prior and likelihood histograms for the last timestep: **a)**  $\pm 0.05 m^3 m^{-3}$  and **b)**  $\pm 0.1 m^3 m^{-3}$  uncertainty ranges.

### Soil Ice Content

The total soil water and liquid water contents were used in Equation (18) to derive the SIC. The resulting average SIC timeseries' and scatter diagrams are given in Figure 24. The model, as depicted by the open loop, underestimated the TSWC and similarly the SIC. The DA updates were able to reduce this with the  $r^2$  being enhanced from 0.54 (OL) to 0.83 ( $\pm 0.05 m^3 m^{-3}$  model uncertainty range) and 0.96 (for the  $\pm 0.1 m^3 m^{-3}$  model uncertainty range).

As with the TSWC updates, the  $\pm 0.1$  uncertainty range provided a fairly broad spread that allowed close tracking of the observed SIC as derived from neutron-inferred average TSWC and averaged USWC from

in-situ sensors. RMSE results similar to the one for TSWC were attained i.e. 0.063, 0.022 and 0.007 for the SFT-OL,  $\pm 0.05 m^3 m^{-3}$  and  $\pm 0.1 m^3 m^{-3}$  model scenarios, respectively.

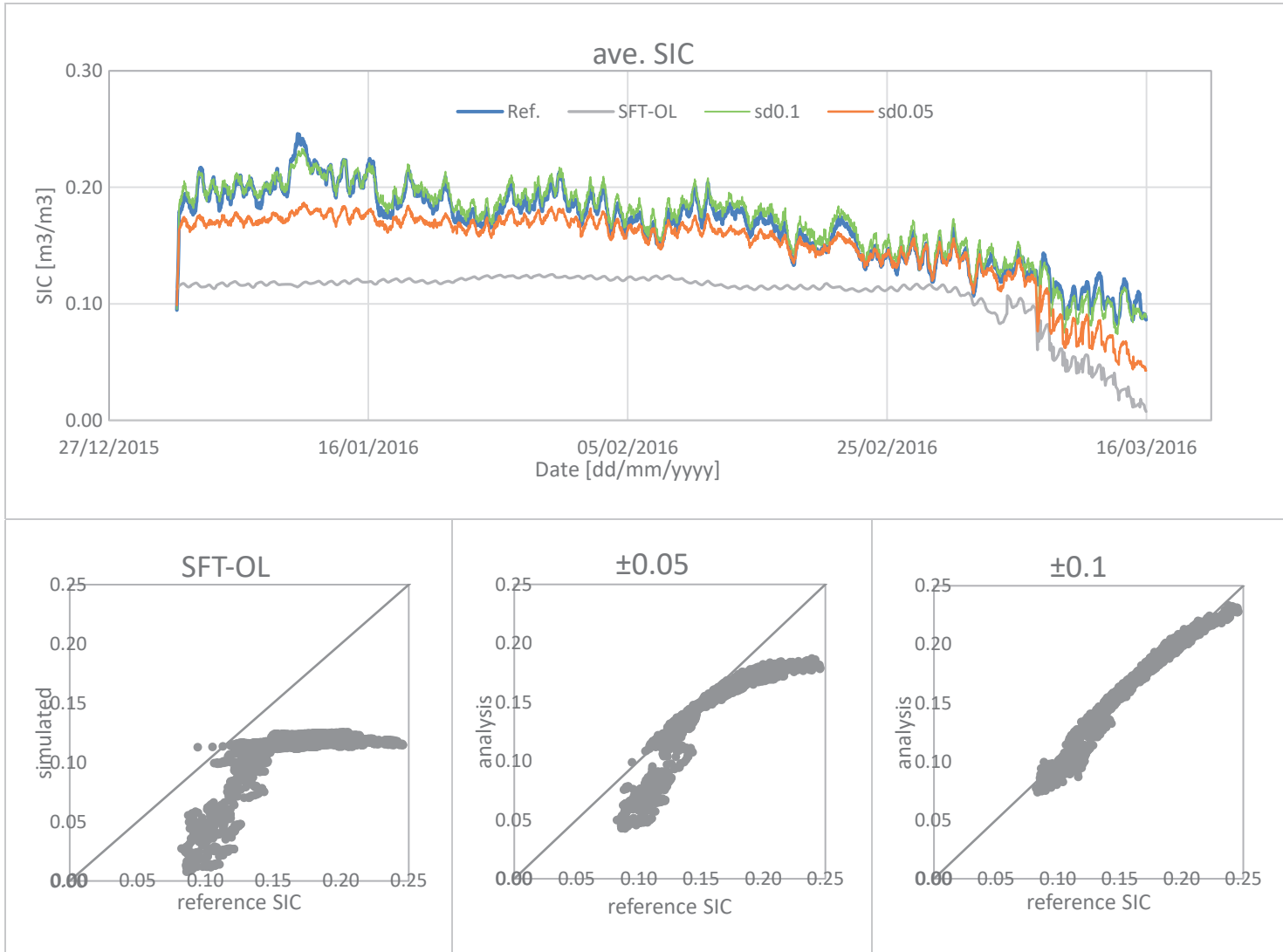


**Figure 24:** Average SIC timeseries (reference, OL and analyses) and respective scatterplots.

In most practical applications, quantification of soil water (in their different phases) over different layers would be preferred to effective depth averages as presented in previous sections. Open loop and updated total, frozen and unfrozen soil water contents over different layers are therefore shown in [Figure 25](#).

The data used to derive the total soil water time series' presented in [Figure 25](#) were obtained from the compiled data pools containing best estimate TSWC analyses (i.e. mean of the posterior ensembles derived from DA implementations). As postulated in sub-section [4.5.2.1](#), the open loop USWC states were left unchanged. Applying Equation (18), the soil ice content data series for the presented layers were consequently derived.

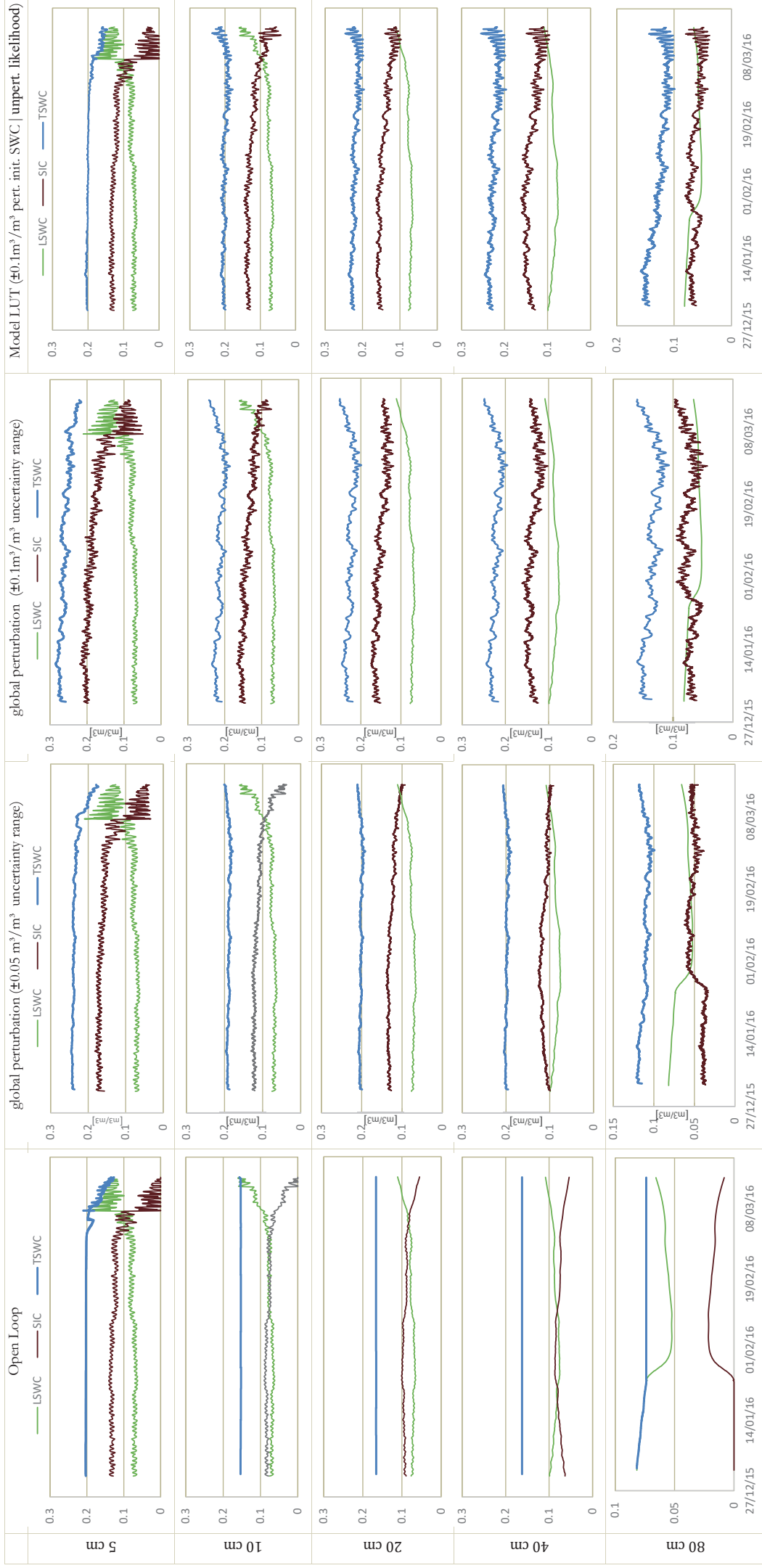
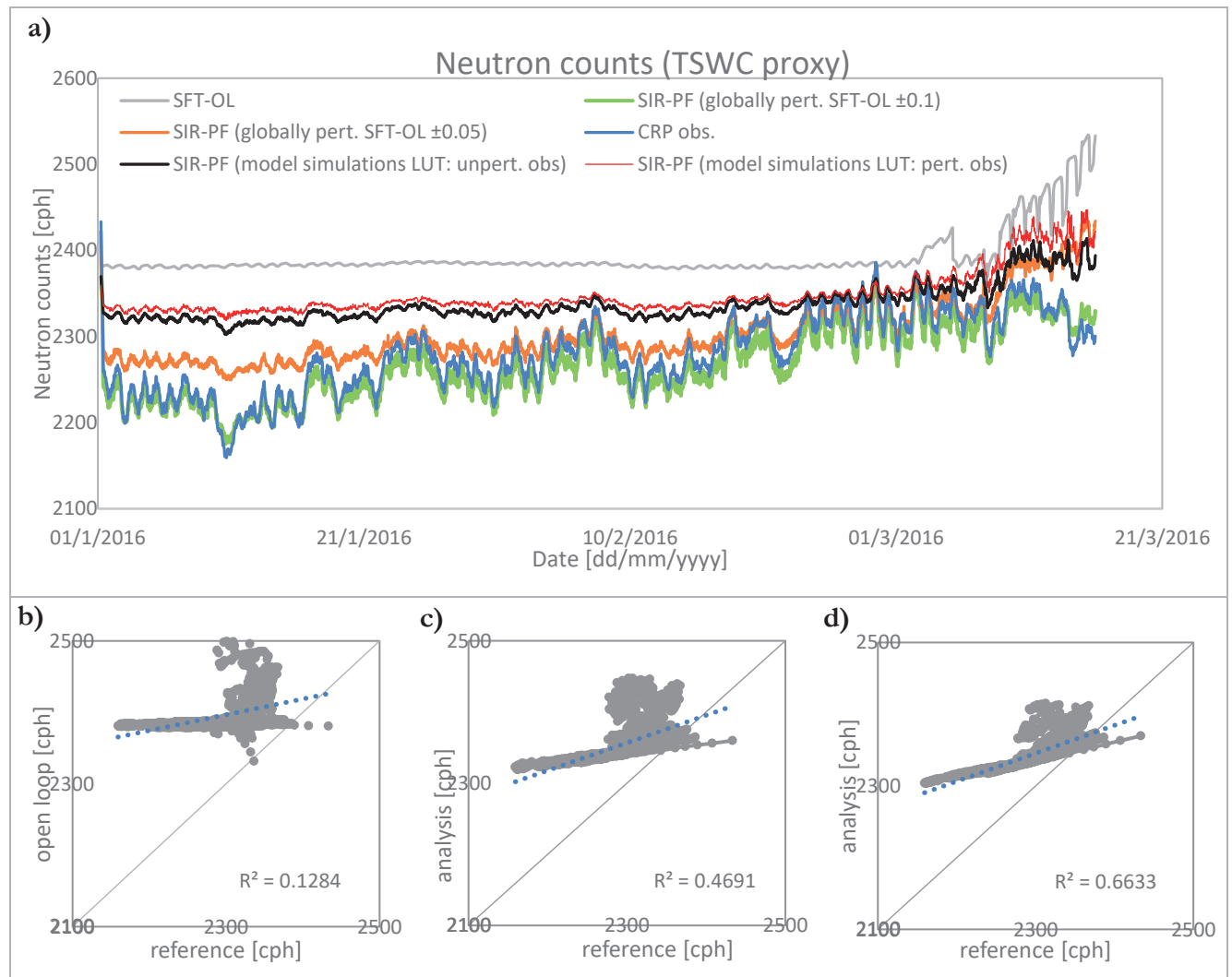


Figure 25: TSWC, USWC and SIC over 5, 10, 20, 40 and 80 cm layers for the different scenarios.

#### 4.5.2.3. Model-derived TSWC Setup (Scenario with LUT precompiled from Model Simulations)

Various tests were performed on the model. The van Genuchten (vG) parameterizations ( $\alpha$  and  $n$ ) were however not changed due to persistent non-convergence of the model. To generate the LUT utilized for this sub-section, the initial SWC content states were perturbed with an uncertainty range of  $\pm 0.1 m^3 m^{-3}$ . The top layer initial SWC was however left unchanged as it also resulted in non-convergence. With each model run for the entire simulation period taking approximately forty (40) minutes, generation of LUTs of ensembles demanded a lot, both in time and computational resources. To attain a reasonable ensemble size, more runs were required to cater for non-converged solutions. A LUT of ensembles with 1004 particles was compiled after enough fully-converged simulation datasets from the model instances were available.

The pre-compiled LUT was then used as the input data pool from which background particles were drawn in a SIR-PF implementation as detailed in [Figure 19](#). Since perturbation of observations led to sharp variations of the analysis estimate, the unperturbed CRP observations (i.e. using unperturbed CRP counts in the PF weighting) were also used to allow for smooth gradients over concurrent updating periods. The resulting timeseries, including the ones already presented in previous sections, are given in [Figure 26](#).



**Figure 26:** **a)** Neutron counts timeseries for analysis utilising LUT model generated particles. Analyses from implementations utilizing LUTs with  $\pm 0.1$  and  $\pm 0.05$  uncertainty ranges added for comparison. Scatter diagrams: **b)** SFT-OL; **c)** model LUT (perturbed likelihood/obs.); **d)** model LUT (unperturbed likelihood/obs.).

The use of unperturbed CRP observations (i.e. where all 1004 likelihood particles for each timestep were set to the observed value) as likelihood against which the prior particles were weighted (see Equation (31)) resulted in a correlation of 0.814. On the other hand, a 0.685 analysis-observation correlation was attained when perturbed CRP measurements were utilized in the PF weighting. An improvement of the shape could also be observed as quantified by the NSE, which was enhanced from -2.021 to 0.274.

The last timestep's histograms as shown in [Figure 27](#) illustrate how these two scenarios result in different best estimates. The rightmost posterior bin appearing with highest frequency (in [Figure 27a](#)) was investigated. It was found that the prior particle with a value of 2517.59 cph was assigned the highest weight in the whole ensemble (i.e. 0.11) even though it was not the prior particle closest to the observation (2300.381cph). This is because the corresponding likelihood particle, against which the weighting was performed, had a value of 2477cph (randomly generated) resulting in a relatively minor ( $y - h(x)$ ) difference in Equation (31) and consequently a higher weight for the particle. A substantial portion of the posterior was henceforth resampled from this prior particle. The same particle was assigned a weight of  $1.18e-5$  in the unperturbed likelihood case. The unperturbed scenario therefore ensured that background particles closest to the observation got the highest weights hence constituting most of the resampled posterior. This particular example shows how the inherent randomness in PFs can at times work against the overall aim of mimicking the observations and also why a large ensemble size is required for the particle filter to be effective.

The timeseries (analyses from perturbed and unperturbed likelihood setups) however overestimate the counts when compared to the  $\pm 0.05 m^3 m^{-3}$  and  $\pm 0.1 m^3 m^{-3}$  uncertainty range scenarios over a large part of the simulated period. This is attributed to the fact that the initial SWC states for the top layer remained unchanged due to convergence issues. Given that top soil layers contribute most to moderation of fast neutrons, underestimation of TSWC in the upper layers reduced the attenuation, consequently resulting in overestimation of simulations by COSMIC.

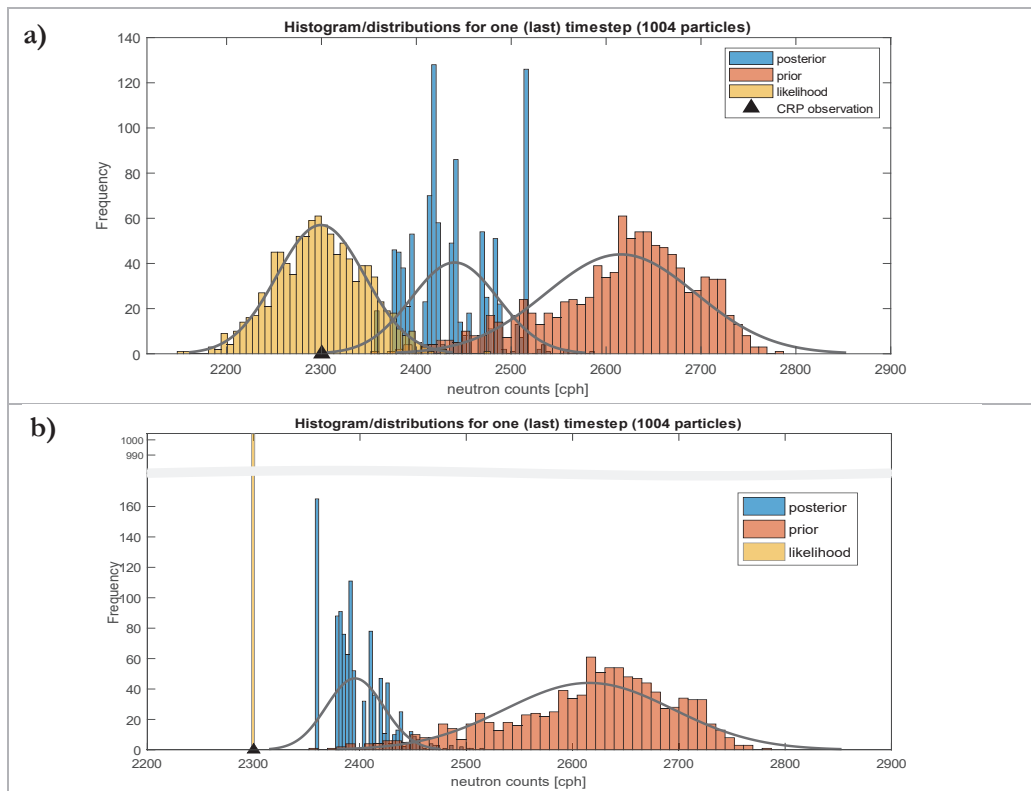


**Figure 27:** Posterior, prior (model simulations LUT; perturbed initial SWC) and likelihood histograms (last timestep). **a)** perturbed and **b)** unperturbed likelihood.

The last timestep's TSWC profiles over the soil column for the different analysis scenarios and SFT-OL are illustrated in [Figure 28](#) below. The scenario with unperturbed likelihood gave a marginally higher soil water profile when compared to the one utilizing perturbed observations.

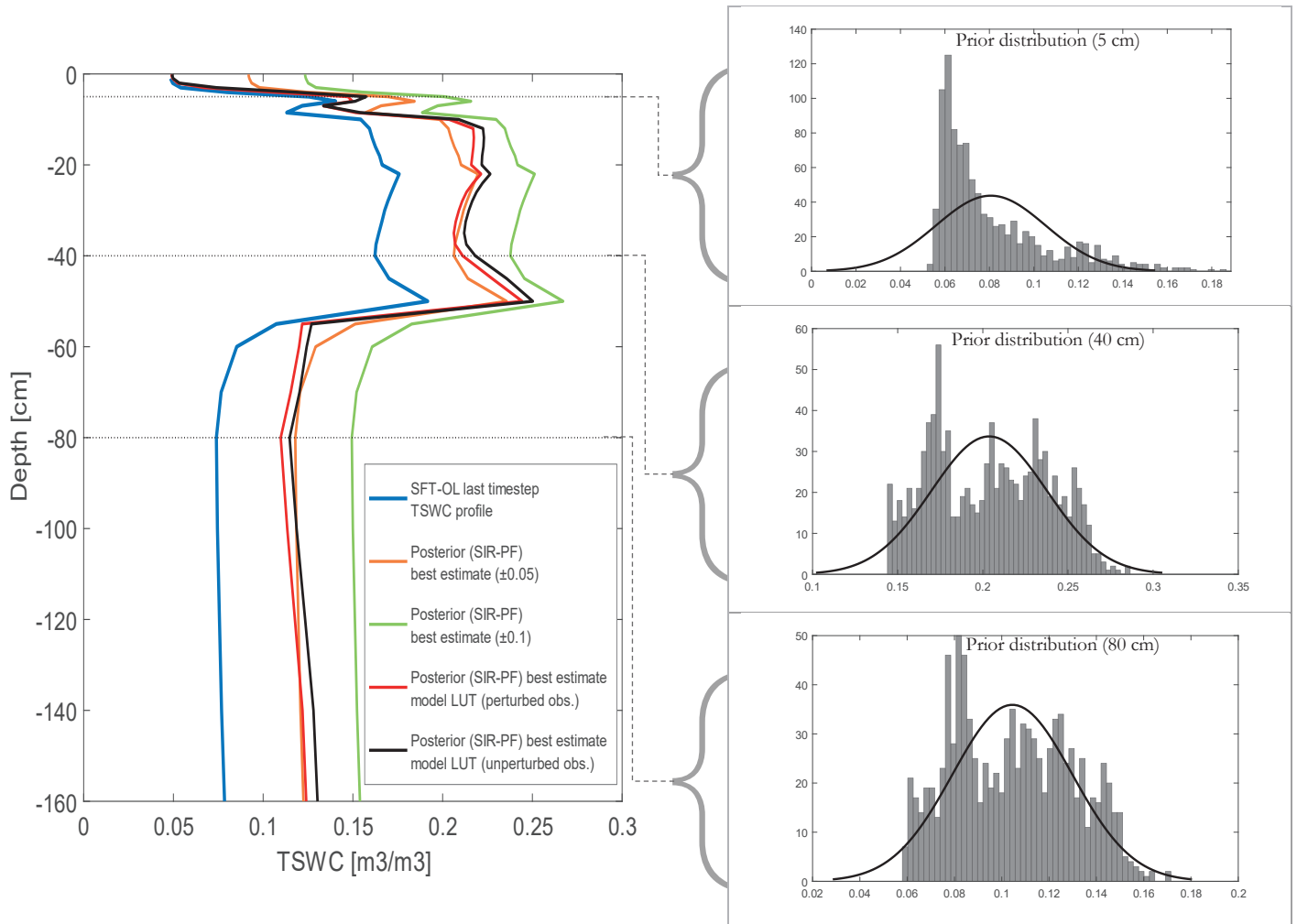


**Figure 28:** Depiction of the last timestep's TSWC profiles under different scenarios (SFT-OL and analyses) and the prior particles distributions/histograms for the 5, 40 and 80 cm soil layers as compiled from model simulations with perturbed initial soil moisture states.

The prior histogram for the 5 cm layer is skewed to the left with most of the particles exhibiting low SWC values. This can also be attributed to the unchanged initial soil moisture in the upper layer propagated over different simulation timesteps although contribution from lower layers seems to result in some of the prior particles having relatively higher values.

For the average TSWC, derived by inputting neutron counts into Equation (14), an RMSE of  $0.036 \text{ m}^3\text{m}^{-3}$  was obtained compared to  $0.041 \text{ m}^3\text{m}^{-3}$  and  $0.061 \text{ m}^3\text{m}^{-3}$  for perturbed likelihood scenario and open loop, respectively. RMSEs for average SIC were  $0.038 \text{ m}^3\text{m}^{-3}$ ,  $0.043 \text{ m}^3\text{m}^{-3}$  and  $0.063 \text{ m}^3\text{m}^{-3}$  for the setups utilizing unperturbed likelihood, perturbed likelihood and open loop, respectively. The total, frozen and unfrozen water content averages over the simulation period for the unperturbed likelihood scenario are therefore illustrated in [Figure 29](#).

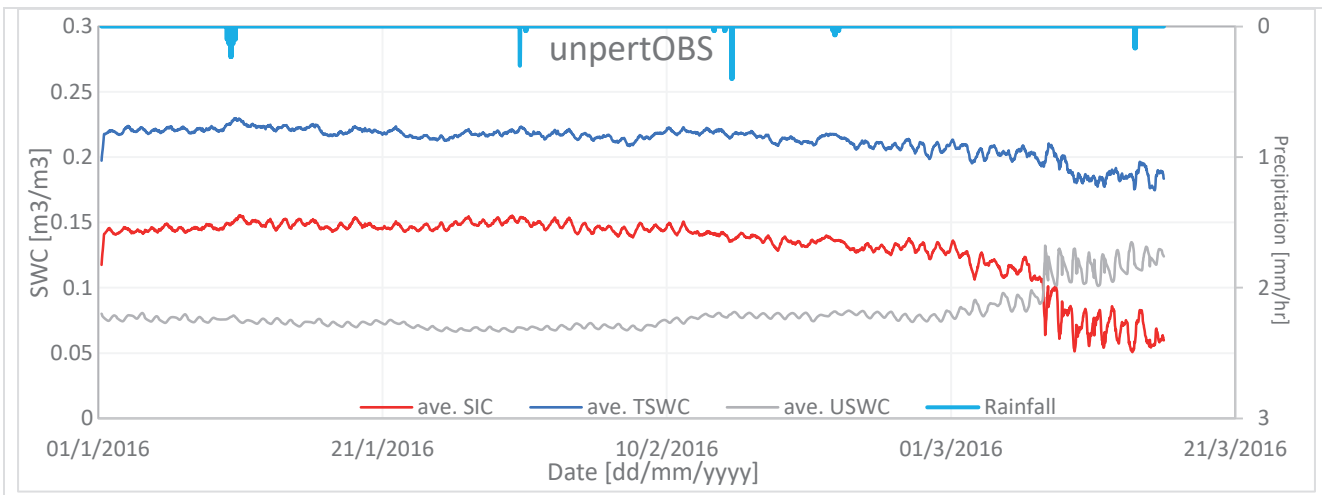


**Figure 29:** Total, frozen and unfrozen average soil water contents. TSWC analysis derived by weighting against unperturbed likelihood in the SIR-PF.

#### 4.6. Limitations

Several aspects limited the scope of this study:

First, it was not feasible, given the available time, to implement the process model in a mode that allowed re-initialization after every timestep. This would have enabled the implementation of the fully coupled SIR-PF scheme as detailed in [Figure 4](#) and hence allow incorporation of other biases such as uncertainties relating to forcing information and model parameters.

Second, dataset from only one in-situ soil moisture was used in investigation and subsequent selection of weighting methods. This is not representative of the spatial heterogeneities, in terms of SM variability, within the cosmic-ray probe footprint. Unlike the sampling campaign data, which were collected from several points in the footprint and thus also included horizontal weighting, the single point (*thus* horizontal weight = 1) SM probe data only allowed vertical weighting. Peng. (2017) also refer to “a small disorder” that “happened during the soil sampling” which could also have influenced the results obtained in this study. Additionally, the sampling campaign only considered a soil column of 40 cm and thus ignored the contribution of deeper layers to the creation and moderation of fast neutrons.

Lastly, it is apparent from the temporal variations of neutron counts that other hydrogen sources, in addition to the already considered soil, lattice and organic water, may have been present during the period under investigation and therefore need to be accounted for. Since no other reference for quantifying the total soil water during the winter period was available, the TSWC inferred from the observed neutron counts was taken as the “truth” without correcting for other hydrogen sources.

## 5. CONCLUSION AND RECOMMENDATIONS

### 5.1. Conclusion

The goal of this study was to improve SIC derivations by assimilating cosmic-ray observations in Maqu, Tibetan plateau. The plausibility of using the uniform averaging approach in calibrating the cosmic-ray probe was first investigated. This was done by comparing the approach to the conventional (both linear and non-linear vertical) and revised weighting methods and validating against weighting by the COSMIC model. The selected weighting approach was then used to average the gravimetric soil moisture datasets collected and compiled by Peng (2017) for recalibrating the CRP. Using the observed neutron counts (TSWC proxy), the tuned site-specific parameter and the in-situ probe (USWC) measurements, the reference (“true”) SIC was derived. The STEMMUS-FT model was then used in assimilation scenarios to derive SIC best estimates. This was done by first compiling data pools that were afterwards used as background datasets in a scheme that utilized the sequential importance resampling – particle filter (SIR-PF) algorithm.

The following could be drawn from analysis of the results:

The use of the equal (uniform) weighting method in calibrating the cosmic ray probe site-specific parameter and in the averaging of soil water in the soil profile was found to be inappropriate as the approach is not based on fast neutrons creation and transport theory. The conventional non-linear averaging method as proposed in Bogen et al. (2013), which was able to assign weights similar to the COSMIC model, was found to be the most suitable and consequently applied.

It was found that with a properly calibrated model, the soil temperature states can accurately be modelled and by applying the tuned soil freezing curve, the unfrozen soil water content simulations could be derived. The total soil water as simulated by the open loop model did not however follow the observed trend as depicted by the cosmic-ray neutron observations.

By applying Bayesian inference, where cosmic-ray neutron observations were assimilated through a particle filter scheme, simulations of total soil water could be improved. This consequently led to improvement of soil ice content simulations given that the model did provide accurate liquid soil water states. The assimilation experiments showed that selection of model uncertainty range to represent various modelling biases (uncertainties in model structure, forcing data, boundary conditions etc.) influenced the outcomes. The  $\pm 0.1m^3m^{-3}$  uncertainty range allowed close tracking of the TSWC observations as inferred from the assimilation results, since it provided enough spread. Use of the data pool compiled from model run simulations also resulted in improvement of simulated counts and thus the TSWC averages although to a smaller extent when compared to the model uncertainties (global perturbation) scenarios. It was also observed that using unperturbed likelihood in the analysis step outperformed use of perturbed observations.

## 5.2. Recommendations

In the particle filter implementation, total soil water particles were drawn from precompiled data pools and propagated through the COSMIC. This method is appropriate for testing the scheme but a fully coupled implementation, where the previous timestep's posterior ensemble members are propagated through STEMMUS for derivation of the current timestep's priors is highly recommended. This will allow addressing other uncertainties inherent in the modelling process i.e. in model parameters, structure, forcing, boundary and initial states information.

As already stated, the observed neutron counts exhibit sharp temporal variations pointing to possible existence of other hydrogen sources. Further work is needed to investigate what these other likely sources are and seek how they can be corrected for (e.g. using the empirical biomass correction approach (Baatz et al., 2015)) to ensure accurate inference of the total soil water. This will also help in reducing the uncertainties calibrating the high energy parameter in the COSMIC model as shown by Baatz et al. (2015). Since the production of fast neutrons depends on soil moisture and soil mineral chemistry (M. Zreda et al., 2012), the effect of the site's mineral composition on the creation and transportation of cosmic-ray fast neutrons could also be investigated. Regarding the use of observations from only one in-situ SM probe in the evaluation and selection of the weighting approach, additional data-series' from within the CRP's footprint could be considered to ensure that soil water spatial heterogeneity is taken into account.

Ideally, it would be better to initially test the DA implementation during a period when total and liquid soil water contents are equivalent (i.e. non-winter periods). This would allow validation of the analyses against in-situ probe SM observations instead of only validating the effective-depth TSWC averages.

## 6. LIST OF REFERENCES

- Baatz, R., Bogena, H. R., Hendricks Franssen, H.-J., Huisman, J. A., Montzka, C., & Vereecken, H. (2015). An empirical vegetation correction for soil water content quantification using cosmic ray probes. *Water Resources Research*, *51*(4), 2030–2046. <https://doi.org/10.1002/2014WR016443>
- Baatz, R., Bogena, H. R., Hendricks Franssen, H.-J., Huisman, J. A., Qu, W., Montzka, C., & Vereecken, H. (2014). Calibration of a catchment scale cosmic-ray probe network: A comparison of three parameterization methods. *Journal of Hydrology*, *516*, 231–244. <https://doi.org/10.1016/j.jhydrol.2014.02.026>
- Beisbart, C., & Norton, J. D. (2013). Why Monte Carlo Simulations Are Inferences and Not Experiments. *International Studies in the Philosophy of Science*, *26*(4), 403–422. <https://doi.org/10.1080/02698595.2012.748497>
- Bogena, H. R., Huisman, J. A., Baatz, R., Hendricks Franssen, H. J., & Vereecken, H. (2013). Accuracy of the cosmic-ray soil water content probe in humid forest ecosystems: The worst case scenario. *Water Resources Research*, *49*(9), 5778–5791. <https://doi.org/10.1002/wrcr.20463>
- Civan, F. (2000). Unfrozen Water in Freezing and Thawing Soils: Kinetics and Correlation. *Journal of Cold Regions Engineering*, *14*(3), 146–156. [https://doi.org/10.1061/\(ASCE\)0887-381X\(2000\)14:3\(146\)](https://doi.org/10.1061/(ASCE)0887-381X(2000)14:3(146))
- Dente, L., Vekerdy, Z., Wen, J., & Su, Z. (2012). Maqu network for validation of satellite-derived soil moisture products. *International Journal of Applied Earth Observation and Geoinformation*, *17*(1), 55–65. <https://doi.org/10.1016/j.jag.2011.11.004>
- Desilets, D., Zreda, M., & Ferré, T. P. A. (2010). Nature's Neutron Probe: Land Surface Hydrology at an Elusive Scale with Cosmic Rays. *Water Resources Research*, *46*(11), 1–7. <https://doi.org/10.1029/2009WR008726>
- Draper, C., Mahfouf, J. F., Calvet, J. C., Martin, E., & Wagner, W. (2011). Assimilation of ASCAT near-surface soil moisture into the SIM hydrological model over France. *Hydrology and Earth System Sciences*, *15*(12), 3829–3841. <https://doi.org/10.5194/hess-15-3829-2011>
- Evensen, G. (1994). Sequential data assimilation with a nonlinear quasi-geostrophic model using Monte Carlo methods to forecast error statistics. *Journal of Geophysical Research*, *99*(C5), 10143–10162. <https://doi.org/doi:10.1029/94JC00572>
- Evensen, G. (2003). The Ensemble Kalman Filter : theoretical formulation and practical implementation. *Ocean Dynamics*, *53*(4), 343–367. <https://doi.org/10.1007/s10236-003-0036-9>
- Famiglietti, J. S., Ryu, D., Berg, A. A., Rodell, M., & Jackson, T. J. (2008). Field Observations of Soil Moisture Variability across Scales. *Water Resources Research*, *44*(1), 1–16. <https://doi.org/10.1029/2006WR005804>
- Franz, T. E., Zreda, M., Ferre, T. P. A., Rosolem, R., Zweck, C., Stillman, S., ... Shuttleworth, W. J. (2012). Measurement depth of the cosmic ray soil moisture probe affected by hydrogen from various sources. *Water Resources Research*, *48*(8), 1–9. <https://doi.org/10.1029/2012WR011871>
- Gordon, N. J., & Salmond, D. J. (1993). Novel approach to nonlinear/non-Gaussian Bayesian state estimation. *IEE Proceedings*, *140*(2), 107–113. <https://doi.org/10.1049/ip-f-2.1993.0015>

- Han, X., Franssen, H. J. H., Rosolem, R., Jin, R., Li, X., & Vereecken, H. (2015). Correction of systematic model forcing bias of CLM using assimilation of cosmic-ray Neutrons and land surface temperature: A study in the Heihe Catchment, China. *Hydrology and Earth System Sciences*, *19*(1), 615–629. <https://doi.org/10.5194/hess-19-615-2015>
- Han, X., Hendricks Franssen, H.-J., Jiménez Bello, M. Á., Rosolem, R., Bogena, H., Alzamora, F. M., ... Vereecken, H. (2016). Simultaneous soil moisture and properties estimation for a drip irrigated field by assimilating cosmic-ray neutron intensity. *Journal of Hydrology*, *539*, 611–624. <https://doi.org/10.1016/j.jhydrol.2016.05.050>
- Hawdon, A., McJannet, D., & Wallace, J. (2014). Calibration and correction procedures for cosmic-ray neutron soil moisture probes located across Australia. *Water Resources Research*, *50*(6), 5029–5043. <https://doi.org/10.1002/2013WR015138>
- Hyndman, R. (2012). How to measure smoothness of a time series in R? - Cross Validated. Retrieved January 31, 2019, from <https://stats.stackexchange.com/q/24610>
- Inaba, H. (1983). Heat Transfer Behavior of Frozen Soils. *Journal of Heat Transfer*, *105*(3), 680–683. <https://doi.org/10.1115/1.3245646>
- Kalman, R. E. (1960). A New Approach to Linear Filtering and Prediction Problems. *Journal of Basic Engineering*, *82*(1), 35–45. <https://doi.org/10.1115/1.3662552>
- Keller, J., Franssen, H. H., & Marquart, G. (2018). Comparing seven variants of the Ensemble Kalman Filter : How many synthetic experiments are needed ? *Water Resources Research*, *54*(9), 6299–6318. <https://doi.org/10.1029/2018WR023374>
- Koopmans, R. W. R., & Miller, R. D. (1966). Soil Freezing and Soil Water Characteristic Curves1. *Soil Science Society of America Journal*, *30*(6), 680–685. <https://doi.org/10.2136/sssaj1966.03615995003000060011x>
- Lakshmi, V. (2014). *Remote Sensing of the Terrestrial Water Cycle*. (V. Lakshmi, D. Alsdorf, M. Anderson, S. Biancamaria, M. Cosh, J. Entin, ... C. Rüdiger, Eds.) (1st ed.). Hoboken, NJ: John Wiley & Sons, Inc. <https://doi.org/10.1002/9781118872086>
- Li, Q., Sun, S., & Xue, Y. (2010). Analyses and development of a hierarchy of frozen soil models for cold region study. *Journal of Geophysical Research*, *115*(D3), 1–18. <https://doi.org/10.1029/2009JD012530>
- Matula, S., Bát'ková, K., & Legese, W. (2016). Laboratory Performance of Five Selected Soil Moisture Sensors Applying Factory and Own Calibration Equations for Two Soil Media of Different Bulk Density and Salinity Levels. *Sensors*, *16*(11), 1912–1934. <https://doi.org/10.3390/s16111912>
- Montzka, C., Moradkhani, H., Weihermüller, L., Franssen, H. J. H., Canty, M., & Vereecken, H. (2011). Hydraulic parameter estimation by remotely-sensed top soil moisture observations with the particle filter. *Journal of Hydrology*, *399*(3–4), 410–421. <https://doi.org/10.1016/j.jhydrol.2011.01.020>
- Montzka, C., Pauwels, V., Franssen, H.-J., Han, X., & Vereecken, H. (2012). Multivariate and Multiscale Data Assimilation in Terrestrial Systems: A Review. *Sensors*, *12*(12), 16291–16333. <https://doi.org/10.3390/s121216291>
- Moradkhani, H. (2008). Hydrologic Remote Sensing and Land Surface Data Assimilation. *Sensors*, *8*(5), 2986–3004. <https://doi.org/10.3390/s8052986>
- Moradkhani, H., DeChant, C. M., & Sorooshian, S. (2012). Evolution of ensemble data assimilation for uncertainty quantification using the particle filter-Markov chain Monte Carlo method. *Water Resources Research*, *48*(12), 1–13. <https://doi.org/10.1029/2012WR012144>

- Moradkhani, H., Hsu, K.-L., Gupta, H., & Sorooshian, S. (2005). Uncertainty assessment of hydrologic model states and parameters: Sequential data assimilation using the particle filter. *Water Resources Research*, *41*(5), 1–17. <https://doi.org/10.1029/2004WR003604>
- Ngodock, H. E., Jacobs, G. A., & Chen, M. (2006). The representer method , the ensemble Kalman filter and the ensemble Kalman smoother : A comparison study using a nonlinear reduced gravity ocean model. *Ocean Modelling*, *12*(3–4), 378–400. <https://doi.org/10.1016/j.ocemod.2005.08.001>
- Owens, R. G., & Hewson, T. (2018). *ECMWF Forecast User Guide*. Reading: ECMWF. <https://doi.org/10.21957/m1cs7h>
- Patterson, D. E., & Smith, M. W. (1981). The measurement of unfrozen water content by time domain reflectometry: results from laboratory tests. *Canadian Geotechnical Journal*, *18*(1), 131–144. <https://doi.org/10.1139/t81-012>
- Pauwels, V. R. N., & Lannoy, J. M. De. (2009). Ensemble-based assimilation of discharge into rainfall-runoff models : A comparison of approaches to mapping observational information to state space. *Water Resources Research*, *45*(8), 1–17. <https://doi.org/10.1029/2008WR007590>
- Peng, J. (2017). *Application of Cosmic-Ray Probe for the Detection of Freezing-Thawing Process over Tibetan Plateau (MSc. Thesis)*. University of Twente. Retrieved from [https://webapps.itc.utwente.nl/librarywww/papers\\_2017/msc/wrem/peng.pdf](https://webapps.itc.utwente.nl/librarywww/papers_2017/msc/wrem/peng.pdf)
- Rosolem, R., Shuttleworth, W. J., Zreda, M., Franz, T. E., Zeng, X., & Kurc, S. A. (2013). The Effect of Atmospheric Water Vapor on Neutron Count in the Cosmic-Ray Soil Moisture Observing System. *Journal of Hydrometeorology*, *14*(5), 1659–1671. <https://doi.org/10.1175/JHM-D-12-0120.1>
- Rowlandson, T. L., Berg, A. A., Bullock, P. R., Ojo, E. R., Mcnairn, H., Wiseman, G., & Cosh, M. H. (2013). Evaluation of several calibration procedures for a portable soil moisture sensor. *Journal of Hydrology*, *498*, 335–344. <https://doi.org/10.1016/j.jhydrol.2013.05.021>
- Savitzky, A., & Golay, M. J. E. (1964). Smoothing and Differentiation of Data by Simplified Least Squares Procedures. *Analytical Chemistry*, *36*(8), 1627–1639. <https://doi.org/10.1021/ac60214a047>
- Schreiner-McGraw, A. P., Vivoni, E. R., Mascaro, G., & Franz, T. E. (2016). Closing the water balance with cosmic-ray soil moisture measurements and assessing their relation to evapotranspiration in two semiarid watersheds. *Hydrology and Earth System Sciences*, *20*(1), 329–345. <https://doi.org/10.5194/hess-20-329-2016>
- Schrön, M., Köhli, M., Scheffele, L., Iwema, J., Bogena, H. R., Lv, L., ... Zacharias, S. (2017). Improving Calibration and Validation of Cosmic-ray Neutron Sensors in the light of Spatial Sensitivity. *Hydrology and Earth System Sciences*, *21*(10), 5009–5030. <https://doi.org/10.5194/hess-21-5009-2017>
- Shuttleworth, J., Rosolem, R., Zreda, M., & Franz, T. (2013). The COsmic-ray Soil Moisture Interaction Code (COSMIC) for use in data assimilation. *Hydrology and Earth System Sciences*, *17*(8), 3205–3217. <https://doi.org/10.5194/hess-17-3205-2013>
- Swinbank, R., & O'Neill, A. (1994). Quasi-biennial and semi-annual oscillations in equatorial wind fields constructed by data assimilation. *Geophysical Research Letters*, *21*(19), 2099–2102. <https://doi.org/10.1029/94GL01743>
- Taylor, K. E. (2001). Summarizing multiple aspects of model performance in a single diagram. *J. Geophys. Res.*, *106*(D7), 7183–7192. <https://doi.org/10.1029/2000JD900719>
- Wösten, J. H. M., Lilly, A., Nemes, A., & Le Bas, C. (1999). Development and use of a database of hydraulic properties of European soils. *Geoderma*, *90*(3–4), 169–185. [https://doi.org/10.1016/S0016-7061\(98\)00132-3](https://doi.org/10.1016/S0016-7061(98)00132-3)

- Yu, L., Zeng, Y., Wen, J., & Su, Z. (2018). Liquid-Vapor-Air Flow in the Frozen Soil. *Journal of Geophysical Research: Atmospheres*, 123(14), 7393–7415. <https://doi.org/10.1029/2018JD028502>
- Zeng, Y. (2013). *Coupled Dynamics in Soil*. (Y. Zeng, Ed.) (1st ed.). Berlin, Heidelberg: Springer Berlin Heidelberg. <https://doi.org/10.1007/978-3-642-34073-4>
- Zeng, Y., Su, Z., Wan, L., & Wen, J. (2011a). A simulation analysis of the advective effect on evaporation using a two-phase heat and mass flow model. *Water Resources Research*, 47(10), 1–18. <https://doi.org/10.1029/2011WR010701>
- Zeng, Y., Su, Z., Wan, L., & Wen, J. (2011b). Numerical analysis of air-water-heat flow in unsaturated soil: Is it necessary to consider airflow in land surface models? *Journal of Geophysical Research Atmospheres*, 116(20), 1–18. <https://doi.org/10.1029/2011JD015835>
- Zhang, H., Franssen, H. J. H., Han, X., Vrugt, J. A., & Vereecken, H. (2017). Joint state and parameter estimation of two land surface models using the ensemble Kalman filter and the particle filter. *Hydrology and Earth System Sciences*, 21(9), 4927–4958. <https://doi.org/10.5194/hess-21-4927-2017>
- Zhao, H., Zeng, Y., Lv, S., & Su, Z. (2018). Analysis of soil hydraulic and thermal properties for land surface modeling over the Tibetan Plateau. *Earth System Science Data*, 10(2), 1031–1061. <https://doi.org/10.5194/essd-10-1031-2018>
- Zreda, M., Desilets, D., Ferré, T. P. A., & Scott, R. L. (2008). Measuring soil moisture content non-invasively at intermediate spatial scale using cosmic-ray neutrons. *Geophysical Research Letters*, 35(21), 1–5. <https://doi.org/10.1029/2008GL035655>
- Zreda, M., Shuttleworth, W. J., Zeng, X., Zweck, C., Desilets, D., Franz, T., & Rosolem, R. (2012). COSMOS: The COsmic-ray Soil Moisture Observing System. *Hydrology and Earth System Sciences*, 16(11), 4079–4099. <https://doi.org/10.5194/hess-16-4079-2012>



## 7. APPENDICES

### Appendix A: Revised weighting parameter functions and constants

Parameter functions as derived by Schrön et al. (2017)

$$F_0 = p_0,$$

$$F_1 = p_0(1 + p_3h)e^{-p_1\theta} + p_2(1 + p_5h) - p_4\theta, \text{ } h \text{ is the absolute air humidity [g m}^{-3}\text{],}$$

$$F_2 = \left( (p_4h - p_0)e^{\frac{-p_1\theta}{1+p_5\theta}} + p_2 \right) (1 + p_3h),$$

$$F_3 = p_0(1 + p_3h)e^{-p_1\theta} + p_2 - p_4\theta,$$

$$F_4 = p_0e^{-p_1\theta} + p_2 - p_3\theta + p_4h,$$

$$F_5 = \left( p_0 - \frac{p_1}{p_2\theta + h - 0.13} \right) (p_3 - \theta)e^{-p_4\theta} - p_5h\theta + p_6,$$

$$F_6 = p_0(h + p_1) + p_2\theta,$$

$$F_7 = (p_0(1 - p_6h)e^{-p_1\theta(1-p_4h)} + p_2 - p_5\theta)(2 + p_3h),$$

$$F_8 = \left( (p_4h - p_0)e^{\frac{-p_1\theta}{1+p_5h+p_6\theta}} + p_2 \right) (2 + p_3h),$$

$$F_p = p_0/(p_1 - e^{-p/1013}), \text{ } p \text{ is the pressure in mbar (hPa),}$$

$F_{veg} = 1 - p_0(1 - e^{-p_1H_{veg}})(1 + e^{-p_2\theta})$ ,  $H_{veg}$  is the vegetation height; a value of 0.2m was assumed in this study.

$r^* = r/F_p/F_{veg}$ ,  $r$  is the distance from the CRP sensor in metres.

Parameter constants as used in the functions are given below;

**Table 6:** Revised weighting parameter constants.

	$p_0$	$p_1$	$p_2$	$p_3$	$p_4$	$p_5$	$p_6$
$F_0$	3.7						
$F_1$	8735	22.689	11720	0.00978	9306	0.003632	
$F_2$	0.027925	6.6577	0.028544	0.002455	$6.851 \cdot 10^{-5}$	12.2755	
$F_3$	247970	23.289	374655	0.00191	258552		
$F_4$	0.054818	21.032	0.6373	0.0791	$5.425 \cdot 10^{-4}$		
$F_5$	39006	15002330	2009.24	0.01181	3.146	16.7417	3727
$F_6$	$6.031 \cdot 10^{-5}$	98.5	0.0013826				
$F_7$	11747	55.033	4521	0.01998	0.00604	3347.4	0.00475
$F_8$	0.01543	13.29	0.01807	0.0011	$8.81 \cdot 10^{-5}$	0.0405	26.74
$F_p$	0.4922	0.86					
$F_{veg}$	0.17	0.41	9.25				
$D_p$	8.321	0.14249	0.96655	0.01	20.0	0.0429	

## Appendix B: Smoothing window sensitivity analysis

Sensitivity analysis on a 20-day dataset (from 01/05/2016 through 20/05/2016) as previously performed by Peng (2017) is illustrated below;

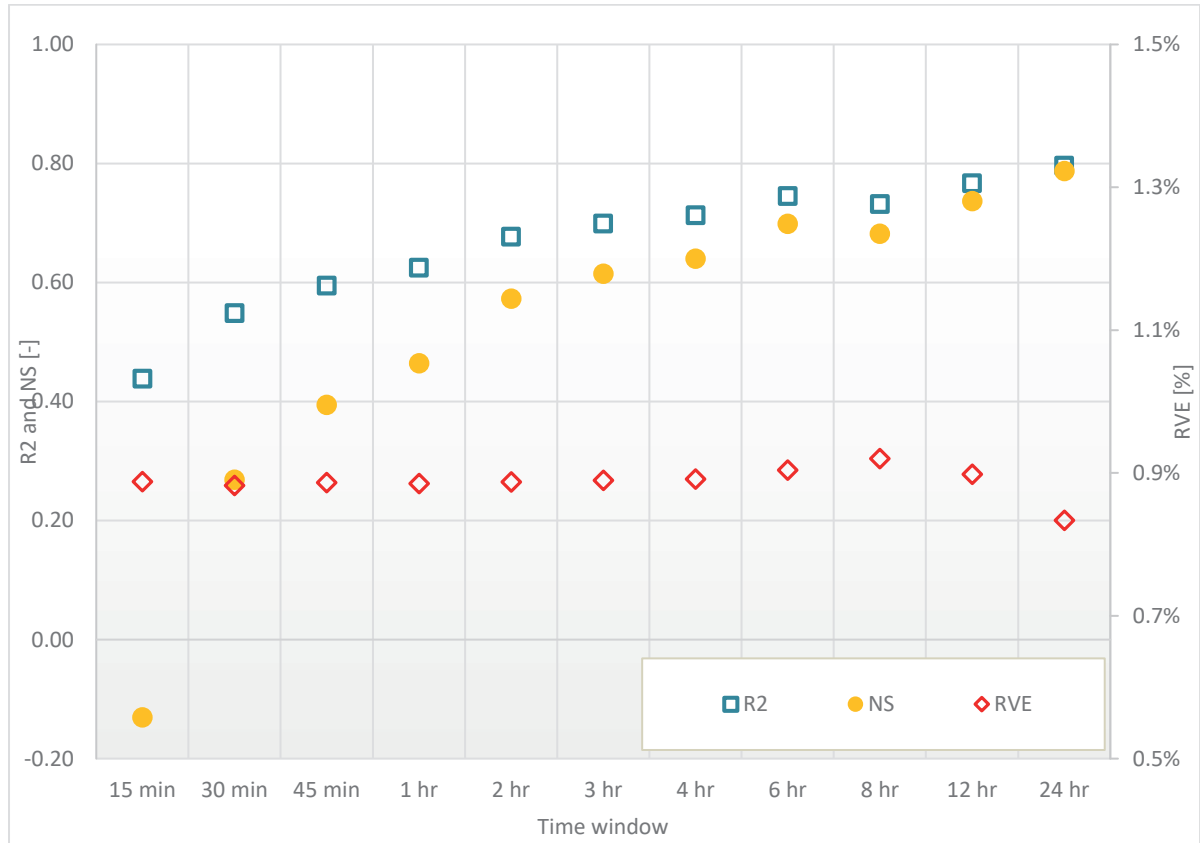


Figure 30: Smoothing window sensitivity analysis based on work by Peng (2017).

Appendix C: COSMIC states only (and state-parameter) DA experiment flow chart

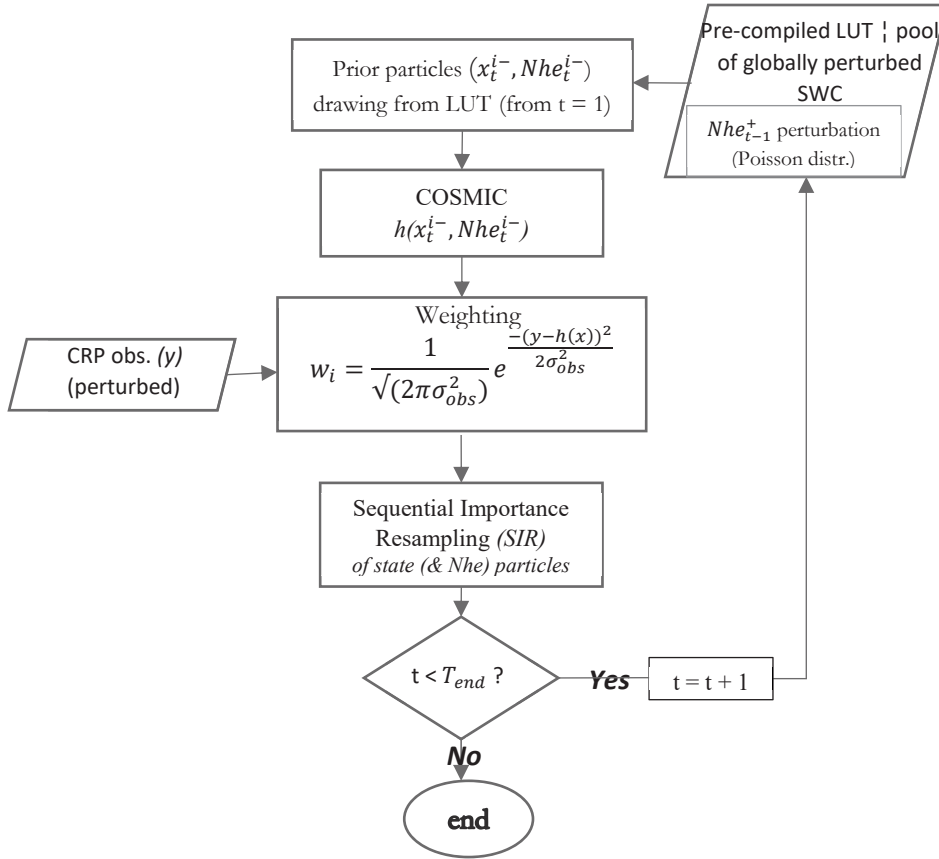


Figure 31: Illustrative COSMIC assimilation experiment.

Appendix D: Observed and Simulated ST timeseries and SFCCs

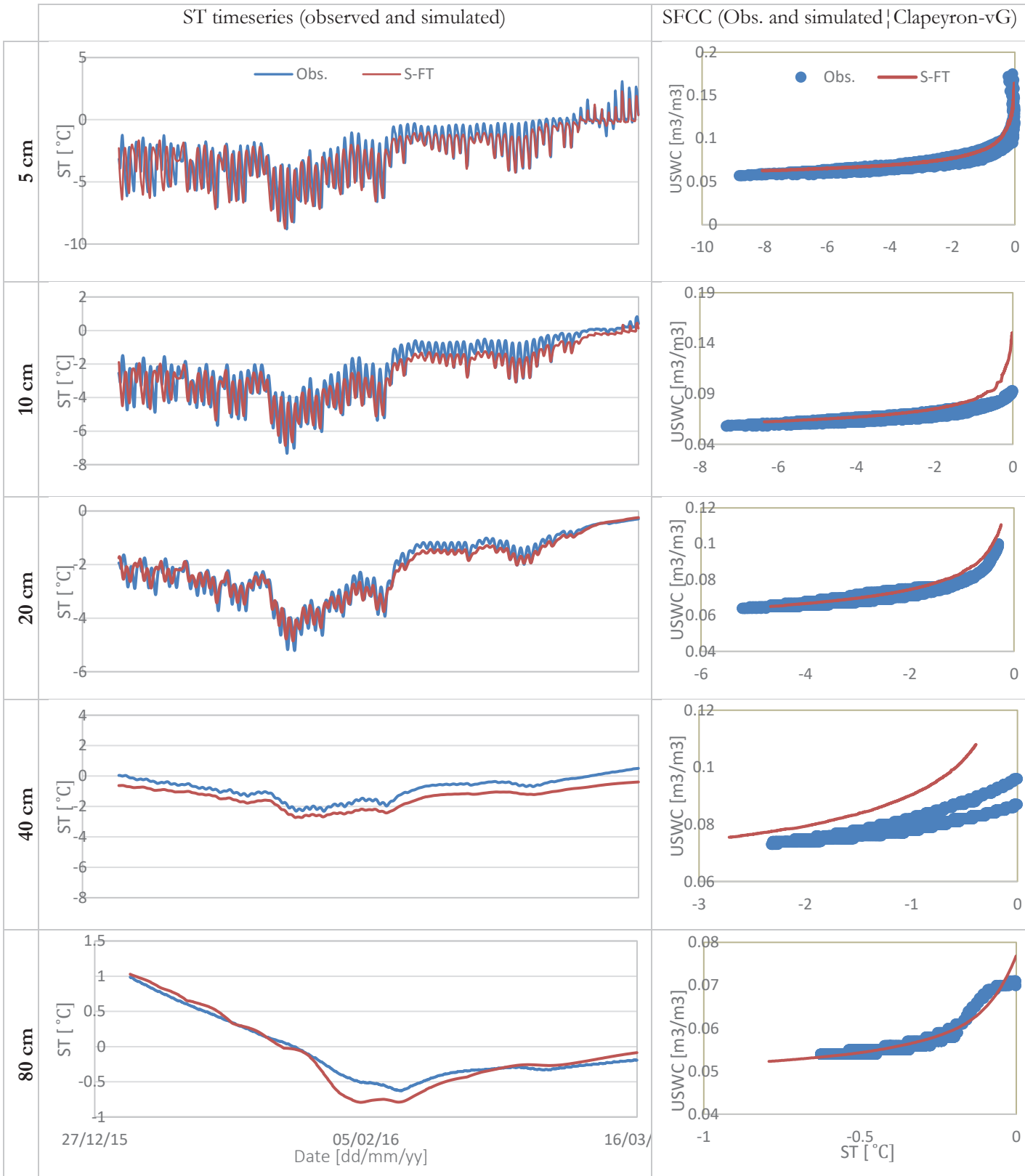
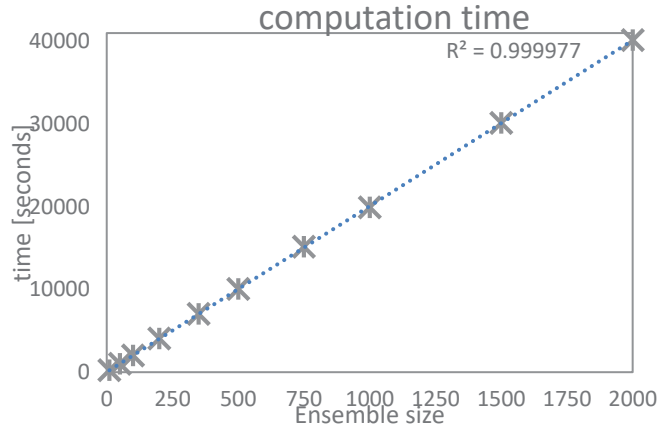


Figure 32: The observed and simulated ST timeseries' and SFCCs over different layers.

## Appendix E: Computational demand and smoothness



**Figure 33:** Computational demand of the SIR-PF utilizing LUTs compiled using  $\pm 0.1 m^3 m^{-3}$  model uncertainty. The LUTs contained 3589 timesteps with varying number of particles.

For a fully coupled DA scheme, significantly higher computation times should be expected because of the integration time that would be required by the numerical process model in its computations.

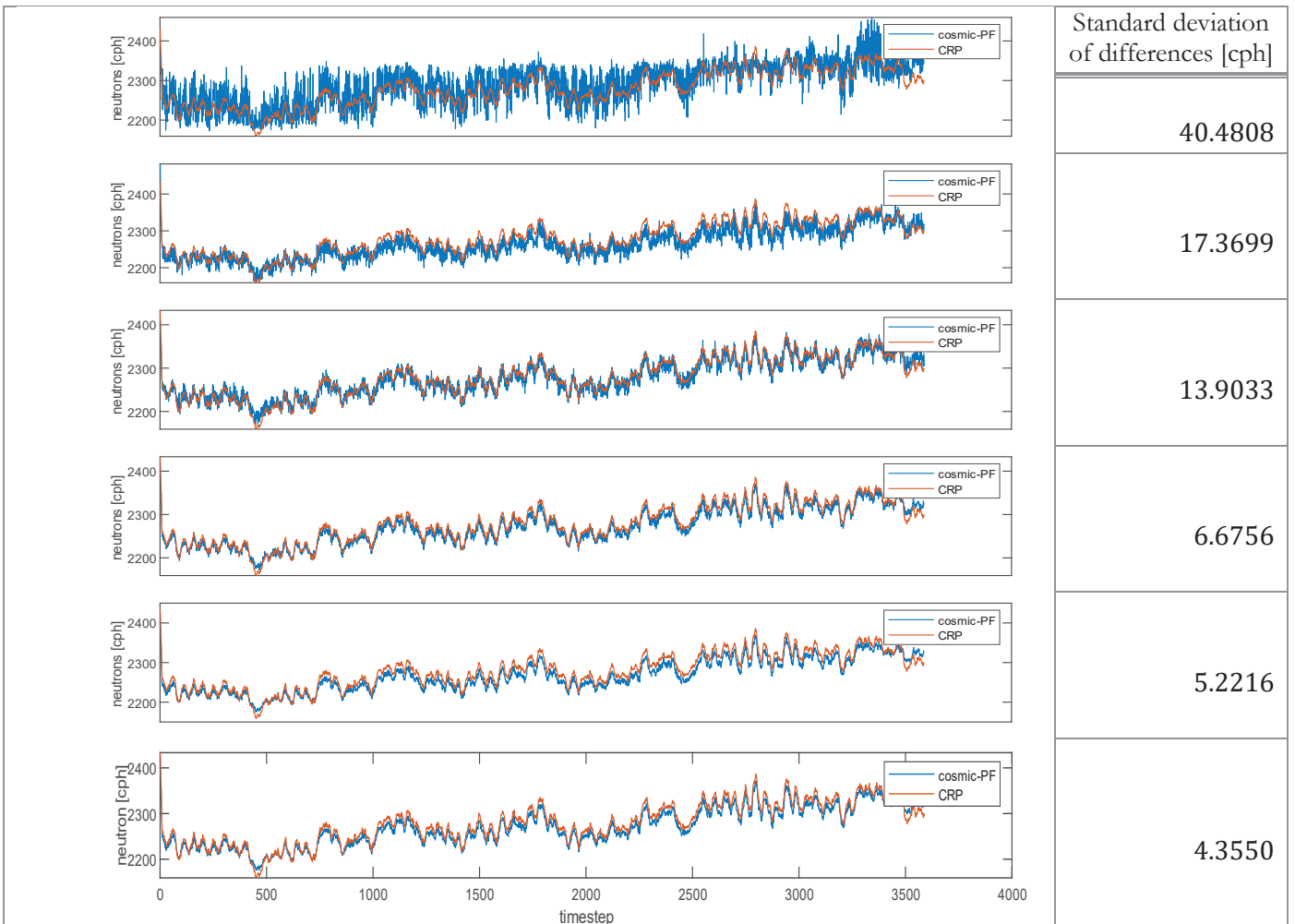


**Figure 34:** Analyses timeseries' obtained from using LUTs (model uncertainty 0.1) with different ensemble members, i.e. from top to bottom: 10, 50, 100, 500, 1000 and 2000 particles, and the corresponding standard deviation of differences (smoothness measure (Hyndman, 2012)).

